Chapter 6
Grinding Science

Mark J. Jackson

Abstract Grinding science is focused on understanding the connectivity between chip formation and the tribology of contact between abrasive grains, bonding agents, fillers, grinding aids and workpiece materials. The chapter reveals information about the nature of real contact by understanding the basic mechanisms of material removal and the nature of sliding contacts during grinding and rubbing of materials. The purpose of this chapter is to provide the reader with: (a) the basic understanding of metal cutting in terms of understanding various plasticity models and by directly observing intimate contact; (b) to explain to the reader the nature of frictional interactions at the machining interface by means of cutting, ploughing and sliding concepts; (c) to explain the effects of frictional heating and lubrication at the contact interface on the ease or difficulty in machining; (d) to provide an analysis of the gaps that are present in the context of the science of grinding: and finally, to provide the reader with a summary of recommendations for stimulate further research activities in order to solve important problems in the area of grinding science.

6.1 Introduction

The basic interactions between grinding wheel and workpiece are commonly associated with cutting, ploughing, sliding, interactions between chip and bond, chip and grain, chip and workpiece, bond sliding against workpiece, chip-to-chip interactions, bond-to-bond interactions, metal-to-metal on grain and chip interactions, interactions with coolants, lubricants (solid and liquid), and grinding aids both active and passive. These interactions may operate in series and/or in parallel and some may not operate at all under the conditions of grinding. Grinding process interactions associated with material removal and tribological processes in the

M.J. Jackson (✉)
Bonded Abrasives Group, Massachusetts Avenue, Cambridge, MA 02139, USA
e-mail: bondedabrasive@gmail.com

J.P. Davim (ed.), *Traditional Machining Processes*,
Materials Forming, Machining and Tribology, DOI 10.1007/978-3-662-45088-8_6

grinding zone are associated with cutting of material by the abrasive grain, material displacement between workpiece and abrasive grain, but without chip formation, surface modification due to frictional effects between abrasive grain and workpiece, interaction between chip and bond, interaction between chip and workpiece, and interaction between bond and workpiece. The current approach to product testing and development is a blend of qualitative and quantitative process analyses. The process interactions explain certain events in a qualitative way, but there is a need to better quantify mechanical, thermal, biological and chemical processes that determine calculated grinding parameters and other metrics that describe abrasive product behaviour, especially when microscopic interactions are dominant during time-dependent behaviours. The importance of power as a function of material removal rate with changes in the threshold power and the level of specific grinding energy explained in terms of which interaction mechanism(s) is(are) operating is necessary to explain the behaviour of the grinding system under certain operating conditions. By observing changes in power as a function of material removal rate, it is not clear which interaction is dominant by way of experimental proof, or whether the observed changes are based on intuition, or not. In this particular case, the issue is the inability to apply existing interaction models to quantitatively explain the change in power as a function material removal in terms of grain wear, bond wear, chip/bond friction, etc. The development of models and new testing and measurement techniques to quantify the effects of various process interactions, or combinations of interactions, on product performance is key to the long-term success and improvement in the abrasive product development cycle.

The purpose of this chapter is to provide the reader with the basic understanding of metal cutting at the microscale in terms of various plasticity models and observations, to explain the nature of frictional interactions at the machining interface including the various cutting, ploughing and sliding interactions, to explain the concept of frictional heating and lubrication at the contact interface, to provide an analysis of the gaps that are present in the context of the science of grinding, and to finally provide the reader with a summary of recommendations for further research activities in order to solve important problems in the area of grinding science.

6.2 Mechanics of Cutting at the Microscale

The purpose of this section of the chapter is to introduce the reader to the mechanics of cutting at the microscale that explains chip formation in terms of material response to an applied force, explains how shear plane angle can be predicted, comments on the plastic behaviour of metals at large strains, and introduces the reader to a number of models that explain metal cutting in terms of material response and develops ‘fluid-like’ features of high strain rate phenomena in metal cutting.

There is a substantial increase in the specific energy required with a decrease in chip size during machining. It is believed this is due to the fact that all metals contain defects such as grain boundaries, missing and/or impurity atoms, stacking faults, etc., and when the size of the material removed decreases the probability of encountering a stress-reducing defect decreases. Since the shear stress and strain in metal cutting is unusually high, discontinuous micro-cracks usually form on the primary shear plane. If the material is very brittle, or the compressive stress on the shear plane is relatively low, micro-cracks will grow into larger cracks giving rise to discontinuous chip formation. When discontinuous micro-cracks form on the shear plane they will weld and reform as strain proceeds, thus joining the transport of dislocations in accounting for the total slip of the shear plane. In the presence of a contaminant, such as carbon tetrachloride vapour at a low cutting speed, the re-welding of micro-cracks will decrease, resulting in a decrease in the cutting force required for chip formation. A number of special experiments that support the transport of micro-cracks across the shear plane, and the important role compressive stress plays on the shear plane are explained. An alternative explanation for the size effect in cutting is based on the belief that shear stresses increase with increasing strain rate. When an attempt is made to apply this to metal cutting, it is assumed in the analysis that the von Mises criterion applies to the shear plane. This is inconsistent with the experimental findings by Merchant. Until this difficulty is resolved with the experimental verification of the strain rate approach, it should be assumed that the strain rate effect may be responsible for some portion of the size effect in metal cutting.

It is known that a size effect exists in metal cutting, where the specific energy increases with decrease in deformation size. Backer et al. [1] performed a series of experiments in which the shear energy per unit volume deformed (u_S) was determined as a function of specimen size for a ductile metal (SAE 1112 steel). The deformation processes involved were as follows, listed from top to bottom with increasing size of specimen deformed: (a) surface grinding; (b) micro milling; (c) turning; and (d) tensile test.

The surface grinding experiments were performed under relatively mild conditions involving plunge type experiments in which an 8-in (20.3 cm) diameter wheel was directed radially downward against a square specimen of length and width 0.5 in (1.27 cm). The width of the wheel was sufficient to grind the entire surface of the work at different down feed rates (t). The vertical and horizontal forces were measured by a dynamometer supporting the workpiece. This enabled the specific energy (u_S) and the shear stress on the shear plane (τ) to be obtained for different values of undeformed chip thickness (t). The points corresponding to a constant specific energy below a value of down feed of about 28 μin (0.7 μm) are on a horizontal line due to a constant theoretical strength of the material being reached when the value of, t, goes below approximately 28 μin (0.7 μm). The reasoning in support of this conclusion is presented in Backer et al. [1].

In the micro milling experiments, a carefully balanced 6-in (152 cm) carbide tipped milling cutter was used with all but one of the teeth relieved so that it operated as a fly milling cutter. Horizontal and vertical forces were measured for a

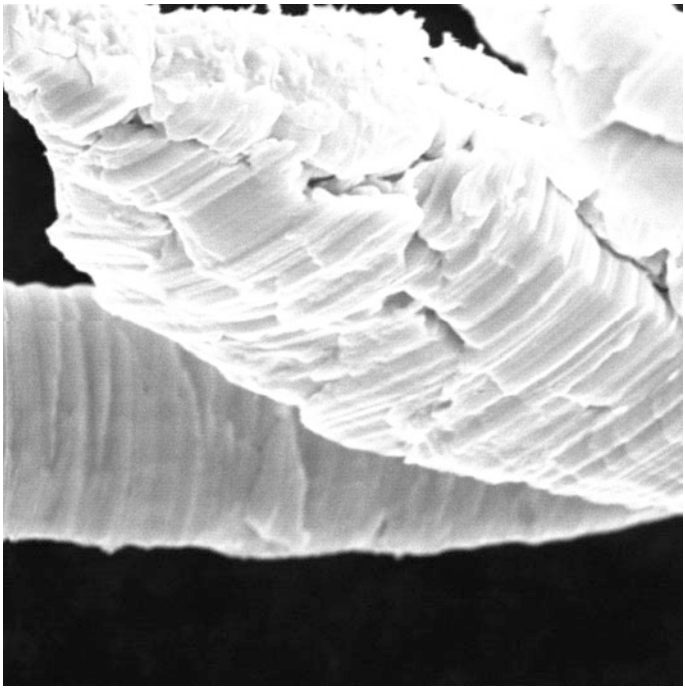

Fig. 6.1 Free surface of chip showing regions of discontinuous strain and microfracture. Reprinted with permission from Jackson and Morrell [31]

number of depths of cut (t) when machining the same sized surface as in grinding. The shear stress on the shear plane (τ) was estimated by a rather detailed method presented in Backer et al. [1]. Turning experiments were performed on a 2.25-in (5.72 cm) diameter SAE 1112 steel bar pre-machined in the form of a thin-walled tube having a wall thickness of 0.2 in (5 mm). A zero degree rake angle carbide tool was operated in a steady-state two-dimensional orthogonal cutting mode as it machined the end of the tube. Values of shear stress on the shear plane (τ) versus undeformed chip thickness were determined for experiments at a constant cutting speed and different values of axial infeed rate and for variable cutting speeds and a constant axial infeed rate.

A true stress-strain tensile test was performed on a 0.505-in (1.28 cm) diameter by 2-in (5.08 cm) gage length specimen of SAE 1112 steel. The mean shear stress at fracture was 22,000 psi (151.7 MPa) [1]. Shaw [2] discusses the origin of the size effect in metal cutting, which is believed to be primarily due to short-range inhomogeneities present in all engineering metals.

When the back of a metal cutting chip is examined at very high magnification by means of an electron microscope individual slip lines are evident as shown in Fig. 6.1. In deformation studies [3] found that slip does not occur on all atomic planes but only on certain discrete planes. In experiments on deformed aluminium

single crystals the minimum spacing of adjacent slip planes was found to be approximately 50 atomic spaces while the mean slip distance along the active slip planes was found to be about 500 atomic spaces. These experiments further support the observation that metals are not homogeneous and suggest that the planes along which slip occurs are associated with inhomogeneities in the metal. Strain is not uniformly distributed in many cases. For example, the size effect in a tensile test is usually observed only for specimens less than 0.1 in (2.5 mm) in diameter. On the other hand, a size effect in a torsion test occurs for considerably larger samples due to the greater stress gradient present in a torsion test than in a tensile test. This effect and several other related ones are discussed in detail by Shaw [2].

6.2.1 Shear Angle Predictions

There have been many notable attempts to derive an equation for the shear angle (ϕ) for steady-state orthogonal cutting. Ernst and Merchant [4] presented the first quantitative analysis. Forces acting on a chip at the tool point where: R = the resultant force on the tool face, R' = the resultant force in the shear plane, N_C and F_C are the components of R normal to and parallel to the tool face, N_S and F_S are the components of R' normal to and parallel to the cutting direction, F_Q and F_P are the components of R normal to and parallel to the cutting direction, and $\beta = \tan^{-1} F_C/N_C$ (is called the friction angle). Assuming the shear stress on the shear plane (τ) to be uniformly distributed it is evident that:

$$\tau = \frac{F_S}{A_S} = \frac{R' \cos(\phi + \beta - \alpha) \sin \phi}{A} \tag{6.1}$$

where A_S and A are the areas of the shear plane and that corresponding to the width of cut (b), times the depth of cut (t). Ernst and Merchant [4] reasoned that τ should be an angle such that τ would be a maximum and a relationship for ϕ was obtained by differentiating Eq. 6.1 with respect to ϕ and equating the resulting expression to zero produces,

$$\phi = 45 - \frac{\beta}{2} + \frac{\alpha}{2} \tag{6.2}$$

However, it is to be noted that in differentiating, both R' and β were considered independent of ϕ. Merchant [5] presented a different derivation that also led to Eq. 6.2. This time an expression for the total power consumed in the cutting process was first written as,

$$P = F_P V = (\tau A V) \frac{\cos(\beta - \alpha)}{\sin \phi \cos(\phi + \beta - \alpha)} \tag{6.3}$$

It was then reasoned that ϕ would be such that the total power would be a minimum. An expression identical to Eq. 6.2 was obtained when P was differentiated with respect to ϕ, this time considering τ and β to be independent of ϕ. Piispanen [6] had done this previously in a graphical way. However, he immediately carried his line of reasoning one step further and assumed that the shear stress τ would be influenced directly by normal stress on the shear plane as follows,

$$\tau = \tau_0 + K_\sigma \tag{6.4}$$

where, K is a material constant. Piispanen [6] then incorporated this into his graphical solution for the shear angle. Upon finding Eq. 6.2 to be in poor agreement with experimental data, Merchant also independently (without knowledge of Piispanen's work at the time) assumed that the relationship given in Eq. 6.4, and proceeded to work this into his second analysis as follows. Hence,

$$\sigma = \tau \tan(\phi + \beta - \alpha) \tag{6.5}$$

or, from Eq. 6.4

$$\tau_0 = \tau + K\tau \tan(\phi + \beta - \alpha) \tag{6.6}$$

Hence,

$$\tau = \frac{\tau_0}{1 - K \tan(\phi + \beta - \alpha)} \tag{6.7}$$

when this is substituted into Eq. 6.3 we have,

$$P = \frac{\tau_0 AV \cos(\beta - \alpha)}{[1 - K \tan(\phi + \beta - \alpha)] \sin\phi \cos(\phi + \beta - \alpha)} \tag{6.8}$$

Now, when P is differentiated with respect to ϕ and equated to zero (with τ_0 and p considered independent of ϕ we obtain,

$$\phi = \frac{\cot^{-1}(K)}{2} - \frac{\beta}{2} + \frac{\alpha}{2} = \frac{C - \beta + \alpha}{2} \tag{6.9}$$

Merchant called the quantity, $\cot^{-1}$ K, the machining "constant" C. The quantity C is seen to be the angle the assumed line relating τ and ϕ makes with the τ axis. Merchant [7] has determined the values of C given in Table 6.1 for materials of different chemistry and structure being turned under finishing conditions with different tool materials. From this table it is evident that C is not a constant. Merchant's empirical machining "constant" C that gives rise to Eq. 6.9 with values of ϕ is in reasonably good agreement with experimentally measured values.

While it is well established that the rupture stress of both brittle and ductile materials is increased significantly by the presence of compressive stress (known as

Table 6.1 Values of C in Eq. 6.9 for a variety of work and tool materials in finish turning without a cutting fluid

Work material	Tool material	C
SAE 1035 Steel	HSS[a]	70
SAE 1035 Steel	Carbide	73
SAE 1035 Steel	Diamond	86
AISI 1022 (leaded)	HSS[a]	77
AISI 1022 (leaded)	Carbide	75
AISI 1113 (sul.)	HSS[a]	76
AISI 1113 (sul.)	Carbide	75
AISI 1019 (plain)	HSS[a]	75
AISI 1019 (plain)	Carbide	79
Aluminium	HSS[a]	83
Aluminium	Carbide	84
Aluminium	Diamond	90
Copper	HSS[a]	49
Copper	Carbide	47
Copper	Diamond	64
Brass	Diamond	74

Reprinted with permission from Jackson and Morrell [31]
[a] *HSS* High-speed steel

the Mohr Effect), it is generally believed that a similar relationship for flow stress does not hold. However, an explanation for this paradox with considerable supporting experimental data is presented below. The fact that this discussion is limited to steady-state chip formation rules out the possibility of periodic gross cracks being involved. However, the role of micro-cracks is a possibility consistent with steady-state chip formation and the influence of compressive stress on the flow stress in shear. A discussion of the role micro-cracks can play in steady-state chip formation is presented in the next section. Hydrostatic stress plays no role in the plastic flow of metals if they have no porosity. Yielding then occurs when the von Mises criterion reaches a critical value. Merchant [5] has indicated that Barrett [8] found that for single crystal metals σ_S is independent of τ_S when plastics such as celluloid are cut. In general, if a small amount of compressibility is involved yielding will occur when the von Mises criterion reaches a certain value.

However, based on the results of Table 6.1 the role of compressive stress on shear stress on the shear plane in steady-state metal cutting is substantial. The fact there is no outward sign of voids or porosity in steady-state chip formation of a ductile metal during cutting and yet there is a substantial influence of normal stress on shear stress on the shear plane represents an interesting paradox. It is interesting to note that Piispanen [6] had assumed that shear stress on the shear plane would increase with normal stress and had incorporated this into his graphical treatment.

6.2.2 Plastic Behaviour at Large Strains

There has been little work done in the region of large plastic strains. Bridgman [9] used hollow tubular notched specimens to perform experiments under combined axial compression and torsion. The specimen was loaded axially in compression as the centre section was rotated relative to the ends. Strain was concentrated in the reduced sections and it was possible to crudely estimate and plot shear stress versus. shear strain with different amounts of compressive stress on the shear plane. From these experiments Bridgman concluded that the flow curve for a given material was the same for all values of compressive stress on the shear plane, a result consistent with other materials experiments involving much lower plastic strains. However, the strain at gross fracture was found to be influenced by compressive stress. A number of related results and possible models are considered in the following subsections.

6.2.2.1 Langford and Cohen's Model

Langford and Cohen [10] were interested in the behaviour of dislocations at very large plastic strains and whether there was saturation relative to the strain hardening effect with strain, or whether strain hardening continued to occur with strain to the point of fracture. Their experimental approach was an interesting and fortunate one. They performed wire drawing on iron specimens using a large number of progressively smaller dies with remarkably low semi die angle (1.5°) and a relatively low (10 %) reduction in area per die pass. After each die pass, a specimen was tested in uniaxial tension and a true stress-strain curve obtained. The drawing and tensile experiments were performed at room temperature and low speeds to avoid heating and specimens were stored in liquid nitrogen between experiments to avoid strain aging effects. All tensile results were plotted in a single diagram, the strain used being that introduced in drawing (0.13 per die pass) plus the plastic strain in the tensile test. The general overlap of the tensile stress-strain curves gives an overall strain-hardening envelope, which indicates that the wire drawing and tensile deformations are approximately equivalent relative to strain hardening [11].

Blazynski and Cole [12] were interested in strain hardening in tube drawing and tube sinking. Drawn tubes were sectioned and tested in plane strain compression. Up to a strain of about 1 the usual strain-hardening curve was obtained that is in good agreement with the generally accepted equation,

$$\sigma = \sigma_1 \varepsilon^n \tag{6.10}$$

However, beyond a strain of 1, the curve was linear corresponding to the equation,

$$\sigma = A + B\varepsilon, (\varepsilon < 1) \tag{6.11}$$

where A and B are constants. It may be shown that,

$$A = (1 - n)\sigma_1 \tag{6.12}$$

$$B = n\sigma_1 \tag{6.13}$$

From transmission electron micrographs of deformed specimens, Langford and Cohen found that cell walls representing concentrations of dislocations began to form at strains below 0.2 and became ribbon shaped with decreasing mean linear intercept cell size as the strain progressed. Dynamic recovery and cell wall migration resulted in only about 7 % of the original cells remaining after a strain of 6. The flow stress of the cold-worked wires was found to vary linearly with the reciprocal of the mean transverse cell size [13].

6.2.2.2 Walker and Shaw's Model

Acoustic studies were performed on specimens of the Bridgman type but fortunately, lower levels of axial compressive stress than Bridgman had used were employed in order to more closely simulate the concentrated shear process of metal cutting. The apparatus used that was capable of measuring stresses and strains as well as acoustic signals arising from plastic flow is described in the dissertation of Walker [14]. Two important results were obtained:

1. A region of rather intense acoustical activity occurred at the yield point followed by a quieter region until a shear strain of about 1.5 was reached. At this point there was a rather abrupt increase in acoustic activity that continued to the strain at fracture which was appreciably greater than 1.5; and
2. The shear stress appeared to reach a maximum at strain corresponding to the beginning of the second acoustic activity ($\gamma \approx 1.5$).

The presence of the notches in the Bridgman specimen made interpretation of stress-strain results somewhat uncertain. Therefore, a new specimen was designed which substitutes simple shear for torsion with normal stress on the shear plane. By empirically adjusting distance Δx to a value of 0.25 mm it was possible to confine all the plastic shear strain to the reduced area, thus making it possible to readily determine the shear strain ($\gamma \approx \Delta y/\Delta x$). When the width of minimum section was greater or less than 0.25 mm, the extent of plastic strain observed in a transverse micrograph at the minimum section either did not extend completely across the 0.25 mm dimension or beyond this width.

Similar results were obtained for non-resulfurised steels and other ductile metals. There is little difference in the curves for different values of normal stress on the shear plane (σ) to a shear strain of about 1.5 [15]. This is in agreement with Bridgman. However, beyond this strain the curves differ substantially with compressive stress on the shear plane. At large strains, τ, was found to decrease with increase in (γ), a result that does not agree with Bridgman [9].

It is seen that for a low value of normal stress on the shear plane of 40 MPa strain hardening appears to be negative at a shear strain of about 1.5; that is, when the normal stress on the shear plane is about 10 % of the maximum shear stress reached, negative strain hardening sets in at a shear strain of about 1.5. On the other hand, strain hardening remains positive to a normal strain of about 8 when the normal stress on the shear plane is about equal to the maximum shear stress.

6.2.2.3 Usui's Model

In Usui et al. [16] an experiment is described designed to determine why CCl_4 is such an effective cutting fluid at low cutting speeds. Since this also has a bearing on the role of micro-cracks in large strain deformation, it is considered here. A piece of copper was prepared. The piece that extends upward and appears to be a chip is not a chip but a piece of undeformed material left there when the specimen was prepared. A vertical flat tool was then placed precisely opposite the free surface and fed horizontally. Horizontal F_P and vertical F_Q forces were recorded as the shear test proceeded. It was expected that the vertical piece would fall free from the lower material after the vertical region had been displaced a small percentage of its length. However, it went well beyond the original extent of the shear plane and was still firmly attached to the base. This represents a huge shear strain since the shear deformation was confined to a narrow band. When a single drop of CCl_4 was placed before the shear test was conducted the protrusion could be moved only a fraction of the displacement in air before gross fracture occurred on the shear plane. Figure 6.2 shows photomicrographs of experiments without and with CCl_4. It is apparent that CCl_4 is much more effective than air in preventing micro-cracks from re-welding.

Saw tooth chip formation for hard steel discussed by Vyas and Shaw [17] is another example of the role micro-cracks play. In this case gross cracks periodically form at the free surface and run down along the shear plane until sufficient compressive stress is encountered to cause the gross crack to change to a collection of isolated micro-cracks.

6.2.3 Fluid-Like Flow in Chip Formation

An interesting paper was presented by Eugene [18]. Water was pumped into a baffled chamber that removed eddy currents and then caused flow under gravity passed a simulated tool. Powdered bakelite was introduced to make the streamlines visible as the fluid flowed passed the tool. The photographs taken by the camera were remarkably similar to quick stop photomicrographs of actual chips. It was thought by this author at the time that any similarity between fluid flow and plastic flow of a solid was not to be expected. That was long before it was clear that the only logical explanation for the results of Bridgman and Merchant involve

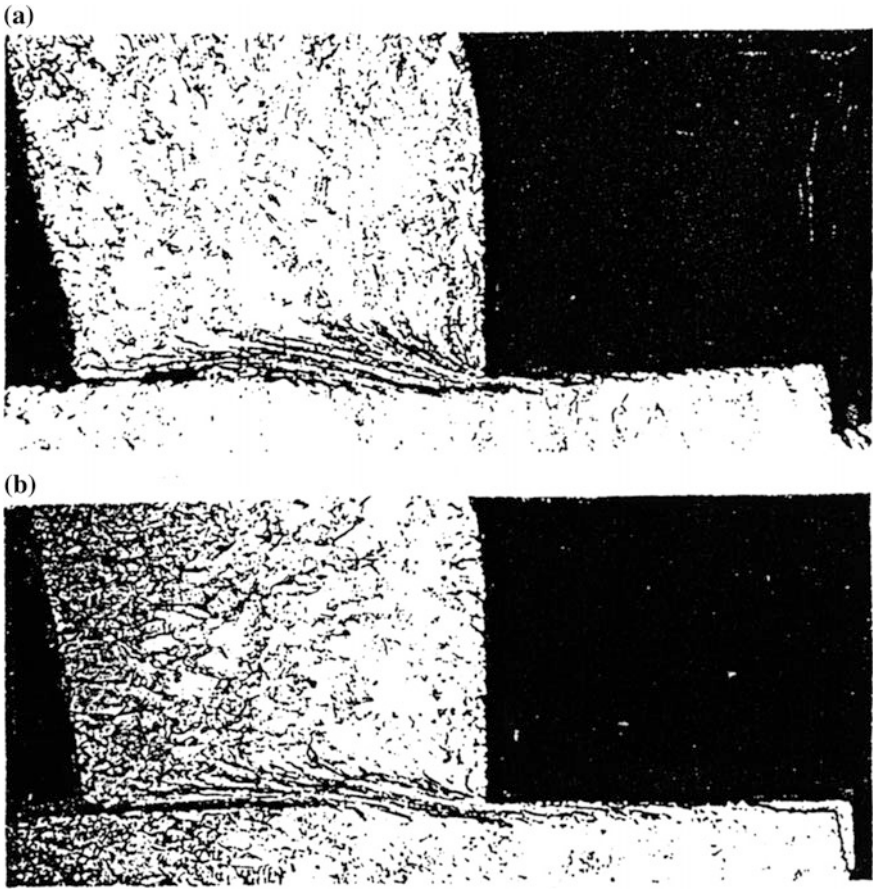

Fig. 6.2 Photomicrographs of specimens that have been sheared a distance approximately equal to the shear plane length: **a** in air; and **b** with a drop of CCl_4 applied. Reprinted with permission from Jackson and Morrell [31]

micro-fracture [19]. A more recent paper was presented that again suggests that metal cutting might be modelled by a fluid [20]. However, this paper was concerned with ultra-precision machining (depths of cut <4 μm) and potential flow analysis was employed instead of the experimental approach taken by Eugene.

It is interesting to note that chemists relate the flow of liquids to the migration of vacancies (voids) just as physicists relate ordinary plastic flow of solid metals to the migration of dislocations. Eyring et al. [21], Eyring and Ree [22], Eyring and Jhon [23] have studied the marked changes in volume, entropy and fluidity that occur when a solid melts. For example, a 12 % increase in volume accompanies melting of Argon, suggesting the removal of every eighth molecule as a vacancy upon melting. This is consistent with X-ray diffraction of liquid argon that showed good short-range order but poor long-range order. The relative ease of diffusion of these

vacancies accounts for the increased fluidity that accompanies melting. A random distribution of vacancies is also consistent with the increase in entropy observed on melting. Eyring's theory of fluid flow was initially termed the *"hole theory of fluid flow"* but later *"The Significant Structure Theory"* [23]. According to this theory the vacancies in a liquid move through a sea of molecules. Eyring's theory of liquid flow is mentioned here since it explains why the flow of a liquid approximates the flow of metal passed a tool in chip formation. In this case micro-cracks (voids) move through a sea of crystalline solid.

6.3 Frictional Interactions at the Machining Interface

Section 6.3 of the chapter focuses on frictional interactions at the machining interface and introduces the reader to understand the mechanics of intimate contact from an experimental viewpoint. Subsections of this viewpoint focus primarily on cutting, ploughing and sliding interactions in terms of static friction and stick-slip phenomena, models for sliding friction, frictional heating and its effect on cutting mechanics, and methods to reduce friction by lubrication.

Initial studies on chip-tool interactions during machining operations were carried out by Professor David Tabor and his team at the Cavendish Laboratory at the University of Cambridge in the United Kingdom during the late 1970s. In their initial studies [24] constructed a transparent sapphire cutting tool bonded to a tool holder that transmitted the action of chip formation so that it could be observed. The reflection of the freshly cut chip is transmitted through the tool by reflecting the image on to a projection face that is highly polished. Doyle et al. [24] reported that they used pure lead and pure tin in air to witness the mechanism of metal transfer to the cutting tool and defined the nature of contact in terms of contact zones as the chip moved across the surface of the tool at low cutting speeds. Initially, two zones were noted, one of sliding across the rake face of the tool (zone 1) and one consisting of the chip material sticking to the rake face (zone 2) ahead of zone 1. On further inspection of the images obtained using a cine camera, zone 1 comprised of two sub zones, namely: zone 1a (where the chip material slides at the edge of the cutting tool on its rake face) and zone 1b (where the chip material sticks to the cutting edge). Further studies by Horne et al. [25], further characterized the nature of contact between the cut chip and the surface of the tool. In an effort to understand the mechanics of chip formation and lubrication, a series of experiments were developed to understand how cooling lubricants provide a thin film between the chip and tool material. In their studies, various lubricants were used and dropped into the chip-tool zone in an effort to provide the means of separation between tool and chip. The lubricant was shown to enter the chip at the side of the material and is absorbed beneath the chip as the chip moves across the rake face. The formation of bubbles is also noticeable when machining aluminium with CCl_4, and may significantly contribute to the change in the mechanism of material transfer from chip to tool or the mechanics of machining. The work currently performed at Purdue

University is based on work that was previously conducted at the Cavendish Laboratory and focuses on quantifying the interactions between chip and tool. This work investigates the applicability of applying orthogonal and oblique cutting theories. The initial work was completed by Madhavan [26]. Again, the use of transparent sapphire tools was employed. The cutting tool has a highly polished surface and was used with a research apparatus that is similar in action to the configuration of a metal planer. A Newport slide, model number PM500-4, was used for the linear slide with which to move the workpiece toward the cutting tool. The slide is controlled by a microprocessor. The velocity of the workpiece ranged from 25 to 150 mm/s. The use of an angle plate was necessary to attach the workpiece to the slide. Another slide was used to adjust the depth of cut of the cutting tool. The entire apparatus was mounted to a vibration isolation table. Soda-lime glass tool was used for comparison with the sapphire tool in order to allow for a comparison of frictional constants and sliding mechanisms between the two substrates. These were again highly polished using small cuboids of soda-lime glass for the rough polish. The final polish involved the use of 1 μm diameter cerium oxide particles. The experiments were imaged using an Olympus model OM-4T microscope. The magnification ranged from ×50 to 200. Force measurements were made with a Kistler piezoelectric transducer. The transducer interestingly enough was configured between the back of the cutting tool and the actual tool holder. The signal produced by the transducer was recorded using an oscilloscope. This was capable of recording the cutting force and the thrust force during machining.

These experiments were conducted for both smooth, polished tools and roughened tools. This was performed to determine if the tool would replicate the rake face of a conventional tool. The tools reflect the image of the rake face to the side of the tool for easy observation as described by Doyle et al. [24]. The initial experiments involved the cutting of wax to develop a basic idea of what may occur. An observation of the process showed that microcracks were formed during the planing of wax. This in turn created a crack along the shear plane. This observation would begin the basis of machining other plastically deformable materials in order to observe the mechanism of machining.

The use of pure lead was considered essential for the experiments concerned with understanding rake face interactions. This was performed using the dry cutting and lubricated conditions. The lubricant was composed of a mixture of 2 parts of oil and 1 part of ink. From these experiments, it was determined that three distinct zones form. The three zones are: Ia, Ib, and II. In zone Ia, the chip interacts with the tool that is known as intimate sliding contact. In zones Ib and II, the chip experiences sticking and metal transfer to the rake face of the tool. When the lubricant is used, metal transfer does not occur in zones Ib and II. It was observed by Doyle et al. [24], that zone II does not form when the experiment is conducted in a vacuum. The idea that there are three distinct zones is puzzling if two of the zones experience the same sliding action. Perhaps two zones with one zone composed of two sub zones would have provided a better explanation of the situation. The magnitude of shear strain is briefly mentioned. The average shear strain for lead is 40–100. The shear strain for aluminium and copper is approximately 20.

There were no calculations included for these values, nor a discussion about the effect of strain causing chip curl. Further experiments were conducted in the later 1990s by Ackroyd [27], who used a new piece of apparatus for characterizing chip-tool interactions. This work further investigated the frictional interactions initially noted by Madhavan [26]. The cutting tool used was again a highly polished sapphire tool bit.

The experimental workpieces used included pure lead as well as pure tin. Both of these materials were obtained from Goodfellow in England. The percentage purity of both materials was 99.95 %. The dimensions of the workpiece were 50 mm^2 × 2 mm thick. Ackroyd [27] also investigated the machining of brass and pure aluminium. Sapphire tools were compared to aluminium and high-speed steel tools. With the use of these tools, a comparative analysis was undertaken to determine if the frictional effects were similar for all tool materials. The sapphire tool was once again polished with cerium oxide and then cleaned with acetone. The rake angles of the tools were 10° and −5°. The experimental apparatus uses a linear drive made by Anorad (model number LW5-750). This unit is capable of a maximum velocity of 2 m/s. The workpiece is similarly mounted to this unit to achieve the maximum workpiece velocity. The vertical stage used was the Newport 433 model. This stage is equipped with the Newport DMH-1, which is a digital micrometer. This allows for measurement of a 1 μm resolution over a 15 mm range. The Newport stage is attached to a Kistler 9254 dynamometer. This is attached to cast iron v-blocks that have been mounted to a worktable. The Kistler unit is used in conjunction with a dual mode amplifier (Kistler 5010B). The optics used for observation can magnify up to ×200. The CCD camera used is a Sony DXC-930. The camera was used in conjunction with s-VHS video. The model used was a Panasonic AG-1970 with a capability of 30 frames per second. The digital high-speed camera used was a Kodak Motion Corder Analyzer Sr-Ultra. It is difficult to determine more than two zones resulting from the machining experiment. For the initial experiments, the following are the parameters were used: The depth of cut was 200 μm; width of cut was 2 mm; length of cut was 50 mm, and the cutting speed ranged from 0.5 to 500 mm/s. It was discovered, and was confirmed by Robinson [28], that the cutting edge plays a significant role in the machining experiments. As the nose radius becomes larger, the depth of cut determines whether the cutting tool cuts, or shears the workpiece material. A large cutting nose radius can create a negative rake angle on the cutting tool if the depth of cut is smaller than the nose radius.

From this work, it can be seen that there are two zones. The first zone involves the chip sliding with no deposit of metal. The second zone involves the chip sticking with some material deposited onto the tool. It was observed that a blunt tool has a higher normal force than a sharp tool. The frictional force versus normal force ratio decreases with the increase in velocity. It was also noted that there were no material deposits to the rake face at higher velocities. The discussion and conclusions of this work show that continual frictional forces increase. This is not a claim that can be substantiated. If frictional force continually increases with friction, it would reach a catastrophic point where the tool would fail. The conclusion was

made using a single machining force measurement to examine both the sticking and sliding regions in question. Both zones cannot be observed simultaneously, therefore a direct comparison cannot be made.

Subsequent work completed by Hwang [29] followed closely the work of Ackroyd [27]. The apparatus that was previously used was upgraded with new components. The use of sapphire and high-speed tools for machining was investigated further by Hwang [29]. The experiments were designed to investigate the sliding and sticking zones. The apparatus was upgraded with a new linear slide. The linear slide was ball screw driven and was supplied by Parker as model number ERB80-B02LAJX-GXS677-A96. This allows for a larger power motor to drive the linear slide. The increased power allowed a larger variety of materials to be investigated. The slide has a maximum speed of 750 mm/s. Again, the vertical stage used was a Newport model number 433. This is actuated using the Newport digital micrometer model number DMH-1. The imaging system remained the same as that used by Ackroyd [27].

A wider variety of plastically deformed materials were used in the experiments. The list includes oxygen free, high conductivity copper (OFHC), cartridge brass, pure lead, Al 1100 aluminium, and Al 6061-T6 aluminium. Hardness values were taken for all materials except for pure lead. The following are the Vickers' hardness values: OFHC = 89.7 kg mm^{-2}, cartridge brass = 153 kg mm^{-2}, Al 1,100 = 49.5 kg mm^{-2}, and Al 6061-T6 = 116 kg mm^{-2}. The workpiece specimens investigated closely were pure lead and Al 6061-T6. The depth of cut for the lead was 200 μm, while the depth of cut for the 6061 was 100 μm. The cutting velocity spanned from 0.5 to 500 mm/s. The exact speeds used were 0.5, 5, 50, and 500 mm/s, respectively. These experiments looked at the effects of lubrication on the chip formation process. The use of lubricant was observed to reduce the length of chip-tool contact length. The investigation focused on the rake face's sliding and sticking regions. This is a continuation of the work performed by Ackroyd [27] and shows the variation in machining different materials. Another aspect of the chip formation process was closely examined. The secondary deformation in a chip was explored with the use of a quick-stop experiment. This is an experiment that stops the cutting tool about three-quarters of the way across the workpiece. This will allow for the examination of the primary shear zone and grain orientation in the chip compared to the substrate. Another segment of the research investigated the use of modulation during machining pure metals with lubricant. The experiment was conducted with a vertical slide as opposed to a horizontal slide. It was not directly observed that the cutting fluid penetrated into the intermittent contact zone during these experiments. This assumption is made due to chip debris remaining static and the elimination of the metal deposit zone. During modulation, frictional forces are much smaller. It was noted that cutting remains under high pressure in the gap ahead of the cutting tool and that the cutting fluid reduced the region of the chip-tool contact. In this region, the contact length reduction promotes a reduction in frictional force. The application of cutting fluid will cause the zone of metal deposits to move further away from the tool edge. This will prevent the expansion of the stagnant metal

zone. This is beneficial to eliminate a partial frictional constant. However, it is questionable as to whether modulation is solely responsible for this action.

The measurement of the rake face temperature was performed using an infra-red imaging system. The signal is reflected at the back of the tool in order to investigate the temperature of the rake face of the tool. The methods of calculating temperature developed by Rapier, Boothroyd, and Loewen and Shaw were used to calculate the rake face temperature. These calculations were then compared to the measured data. From these results, it can be reasoned that modulation does not solve the frictional contact problem. However, modulation does create a constant cutting length and constant values of friction between chip and tool. However, this action alone is dependent upon the stroke length chosen, and will be different for each material machined and the corresponding depth of cut.

The research conducted by Lee [30] follows closely the work of both Ackroyd [27] and Hwang [29]. Lee's study included using particle image velocimetry to measure chip velocity. This utilized a linear slide with a ball screw and allows for an adjustment of the depth of cut as little as 1 μm. A charge-coupled device (CCD) was used for high-speed imaging. Similar to the Hwang's work, a Kodak Motion Corder Analyzer Sr-Ultra was used. An optical microscope records the chip formation process, and employs a Nikon Optiphot that can examine the specimen up to ×200 magnification. The CCD can capture images of up to 10,000 fps using a black and white format. The spatial resolution is 3.3 μm pixel size. The experiments were conducted dry. The workpiece specimens used were commercially pure lead and copper that is 99.95 % pure. These were both obtained from Goodfellow, UK. In the initial investigation using 6061-T6 aluminium, a built-up edge (BUE) was observed on the rake face. The BUE changes the rake angle thus increasing the chip velocity more than in the machining of other materials.

The velocity of the chip was inspected using constrained workpiece specimens. These areas show the rake face and the side view of the cut chip. This allows for the investigation of the metal deposit on the rake face and the effects of deformation in the secondary zone. A vertical stage moves the tool into contact with the workpiece. This is made possible through the use of a micrometer. At the foundation is the ball screw drive that brings the workpiece into contact with the cutting tool. This is a satisfactory experimental apparatus. However, there remains much to be desired with this particular apparatus in terms of rigidity and range of workpiece cutting speeds.

6.3.1 Cutting, Ploughing and Sliding Interactions

The nature of the contact between surfaces is an important aspect of understanding the function of tribology in machining [31]. The properties of the materials in contact are homogeneous and isotropic. Macro-contact conditions are most useful in models for friction when there is lubrication and the effects of surface heterogeneities are of little importance. Hertz's equations allow engineers to calculate the

Table 6.2 Equations for calculating elastic (Hertz) contact stress

Symbol	Definition
P	Normal force
p	Normal force per unit contact length
$E_{1,2}$	Modulus of elasticity for bodies 1 and 2, respectively
$\nu_{1,2}$	Poisson's ratios for bodies 1 and 2, respectively
D	Diameter of the curved body, if only one if curved
$D_{1,2}$	Diameters of bodies 1 and 2, where $D_1 > D_2$ by convention
S_c	Maximum compressive stress
a	Radius of the elastic contact
b	Width of a contact (for cylinders)
E*	Composite modulus of bodies 1 and 2
A, B	Functions of the diameters of bodies 1 and 2

Geometry	Contact dimension	Contact stress
Sphere-on-flat	$a = 0.721\sqrt{[3]PDE^*}$	$S_c = 0.918\sqrt{[3]P/(D^2E^*)^2}$
Cylinder-on-flat	$b = 1.6\sqrt{pDE^*}$	$S_c = 0.798\sqrt{p/DE^*}$
Cylinder-on-cylinder (axes parallel)	$b = 1.6\sqrt{pE*/A}$	$S_c = 0.798\sqrt{pA/E*}$
Sphere in a spherical socket	$a = 0.721\sqrt{[3]PE*/B}$	$S_c = 0.918\sqrt{[3]P(B/E*)^2}$
Cylinder in a circular groove	$b = 1.6\sqrt{pE*/B}$	$S_c = 0.798\sqrt{pB/E*}$

Reprinted with permission from Jackson and Morrell [31]

maximum compressive contact stresses and contact dimensions for non-conforming bodies in elastic contact. The parameters required to calculate the quantities and the algebraic equations used for simple geometries are given in Table 6.2 [32]. It should be noted that Hertz's equations apply to static, or quasi-static, elastic cases. In the case of sliding, plastic deformation, contact of very rough surfaces, or significant fracture, both the distribution of stresses and the contact geometry will be altered. Hertz's contact equations have been used in a range of component design applications, and in friction and wear models in which the individual asperities are modeled as simple geometric contacts.

Greenwood and Williamson [33] developed a surface geometry model that modeled contacts as being composed of a distribution of asperities. From that assumption, contact between such a surface and a smooth, rigid plane could be determined by three parameters: the asperity radius (R), the standard deviation of asperity heights (σ^*), and the number of asperities per unit area. To predict the extent of the plastic deformation of asperities, the plasticity index (ψ), also a function of the hardness (H), elastic modulus (E), and Poisson's ratio (ν), was introduced.

$$\psi = \left(\frac{\mathrm{E}'}{\mathrm{H}}\right)\left(\frac{\sigma*}{R}\right)^{1/2} \tag{6.14}$$

where, $E' = E/(1-\nu^2)$. This basic formulation was refined by various investigators such as Whitehouse and Archard [34] to incorporate other forms of height distributions, and the incorporation of a distribution of asperity radii, represented by the correlation distance β*, which produced higher contact pressures and increased plastic flow. Therefore,

$$\psi = \left(\frac{E'}{H}\right)\left(\frac{\sigma*}{\beta}\right)^{1/2} \tag{6.15}$$

Hirst and Hollander [35] used the plasticity index to develop diagrams to predict the start of scuffing wear. Other parameters, such as the average or root mean square slope of asperities, have been incorporated into wear models to account for such peculiarities [36]. Worn surfaces are observed to be much more complex than simple arrangements of spheres, or spheres resting on flat planes, and Greenwood readily acknowledged some of the problems associated with simplifying assumptions about surface roughness [37]. A comprehensive review of surface texture measurement methods have been given by Song and Vorburger [38]. The most commonly used roughness parameters are listed in Table 6.3. Parameters such as skewness are useful for determining lubricant retention qualities of surfaces, since they reflect the presence of cavities. However, one parameter alone cannot precisely model the geometry of surfaces. It is possible to have the same average roughness (or RMS roughness) for two different surfaces.

Small amounts of wear can change the roughness of surfaces on the microscale and disrupt the nanoscale structure as well. Some of the following quantities have been used in models for friction:

1. The true area of contact;
2. The number of instantaneous contacts comprising the true area of contact;
3. The typical shapes of contacts (under load);
4. The arrangement of contacts within the nominal area of contact; and
5. The time needed to create new points of contact.

Finally, contact geometry-based models for friction generally assume that the normal load is constant. This assumption may be unjustified, especially when sliding speeds are relatively high, or when there are significant friction and vibration interactions in the tribosystem. As the sliding speed increases, frictional heating increases and surface thermal expansion can cause intermittent contact. The growth and excessive wear of intermittent contact points is termed thermoelastic instability (TEI) [39]. TEI is only one potential source of the interfacial dynamics responsible for stimulating vibrations and normal force variations in sliding contacts. Another major cause is the eccentricity of rotating shafts, run-out, and the transmission of external vibrations. Static friction and stick-slip behaviour are

Table 6.3 Definitions of surface roughness parameters

Let y_i = vertical distance from the ith point on the surface profile to the mean line	
N = number of points measured along the surface profile	
Thus, the following are defined:	
Arithmetic average roughness	$R_a = \frac{1}{N}\sum_{i=1}^{N}\lvert y_i\rvert$
Root-mean-square roughness	$R_q = \left[\frac{1}{N}\sum_{i=1}^{N} y_i^2\right]^{1/2}$
Skewness	$R_{sk} = \frac{1}{NR_q^3}\sum_{i=1}^{N} y_i^3$
	A measure of the symmetry of the profile
	R_{sk} = 0 for a Gaussian height distribution
Kurtosis	$R_{kurtosis} = \frac{1}{NR_q^4}\sum_{i=1}^{N} y_i^4$
	A measure of the sharpness of the profile
	$R_{kurtosis}$ = 3.0 for a Gaussian height distribution
	$R_{kurtosis}$ < 3.0 for a broad distribution of heights
	$R_{kurtosis}$ > 3.0 for a sharply-peaked distribution

Reprinted with permission from Jackson and Morrell [31]

considered, and as with kinetic friction, the causes for such phenomena can be interpreted on several scales.

6.3.1.1 Static Friction and Stick-Slip Phenomena

If all possible causes for friction are to be considered, it is reasonable to find out whether there are other means to cause bodies to stay together without the requirement for molecular bonding. Surfaces may adhere, but adherence is not identical to adhesion, because there is no requirement for molecular bonding. If a certain material is cast between two surfaces and, after penetrating and filling irregular voids in the two surfaces, solidifies to form a network of interlocking contacting points there may be strong mechanical joint produced, but no adhesion. Adhesion (i.e., electrostatically balanced attraction/chemical bonding) in friction theory meets the need for an explanation of how one body can transfer shear forces to another. Clearly, it is convenient to assume that molecular attraction is strong enough to allow the transfer of force between bodies, and in fact this assumption has led to many of the most widely used friction theories. From another perspective, is it not equally valid to consider that if one pushes two rough bodies together so that asperities penetrate, and then attempts to move those bodies tangentially, the atoms may approach each other closely enough to repel strongly, thus causing a backlash against the bulk materials and away from the interface. The repulsive force parallel to the sliding direction must be overcome to move the bodies tangentially,

whether accommodation occurs by asperities climbing over one another, or by deforming one another. In the latter, it is repulsive forces and not adhesive bonding that produces sliding resistance. This section focuses on static friction and stick slip phenomena.

Ferrante et al. [40] have provided a comprehensive review of the subject. A discussion of adhesion and its relationship to friction has been conducted by Buckley [41]. Atomic probe microscopes permit investigators to study adhesion and lateral forces between surfaces on the atomic scale. The force required to shift the two bodies tangentially must overcome bonds holding the surfaces together. In the case of dissimilar metals with a strong bonding preference, the shear strength of the interfacial bonds can exceed the shear strength of the weaker of the two metals, and the static friction force ($\mathbf{F}_s$) will depend on the shear strength of the weaker material (τ_m) and the area of contact (A). In terms of the static friction coefficient μ_s,

$$\mathbf{F}_s = \mu_s \, \mathbf{P}* = \tau_m A \tag{6.16}$$

or,

$$\mu_s = (\tau_m / \mathbf{P}*) A \tag{6.17}$$

where $\mathbf{P}*$, the normal force is comprised of the applied load and the adhesive contribution normal to the interface. Under specially controlled conditions, such as friction experiments with clean surfaces in vacuum, the static friction coefficients can be greater than 1.0, and the experiment becomes a test of the shear strength of the solid materials than of interfacial friction. Scientific understanding and approaches to modeling friction has been strongly influenced by concepts of solid surfaces and by the instruments available to study them. Atomic-force microscopes and scanning tunneling microscopes permit views of surface atoms with high resolution and detail. Among the first to study nanocontact frictional phenomena were McClellan et al. [42, 43]. A tungsten wire with a very fine tip is brought down to the surface of a highly oriented, cleaved basal plane of pyrolytic graphite as the specimen is oscillated at 10 Hz using a piezoelectric driver system. The cantilevered wire is calibrated so that its spring constant is known (2,500 N/m) and the normal force could be determined by measuring the deflection of the tip using a reflected laser beam. As the normal force is decreased, the contributions of individual atoms to the tangential force became apparent. At the same time, it appeared that the motion of the tip became less uniform, exhibiting atomic-scale stick-slip.

Thompson and Robbins [44] discussed the origins of nanocontact stick-slip when analyzing the behaviour of molecularly thin fluid films trapped between flat surfaces of face-centered cubic solids. At that scale, stick-slip was believed to arise from the periodic phase transitions between ordered static and disordered kinetic states. Immediately adjacent to the surface of the solid, the fluid assumed a regular, crystalline structure, but this was disrupted during each slip event. The experimental data points of friction force per unit area versus time exhibited extremely uniform classical stick-slip appearance. Once slip occurred, all the kinetic energy must be

converted into potential energy in the film. In subsequent papers [45] this group of authors used this argument to calculate the critical velocity, $v_{c,}$ below which the stick-slip occurs is:

$$v_c = c(\sigma \mathbf{F}_s/M)^{1/2} \tag{6.18}$$

where σ is the lattice constant of the wall, $\mathbf{F}_s$ is the static friction force, M is the mass of the moving wall, and c is a constant.

Friction is defined as the resistance to relative motion between two contacting bodies parallel to a surface that separates them. Motion at the atomic scale is unsteady. In nanocontact, accounting for the tangential components of thermal vibrations of the atoms thus affects our ability to clearly define relative motion between surfaces. Under some conditions it may be possible to translate the surface laterally while the adhesive force between the probe tip and the opposite surface exceeds the externally applied tensile force. Landman et al. [46] reviewed progress in the field of molecular dynamics (MD). By conducting MD simulations of nickel rubbing a flat gold surface, Landman illustrated how the tip can attract atoms from the surface simply by close approach without actual indentation. A connective neck or bridge of surface atoms was observed to form as the indenter was withdrawn. The neck can exert a force to counteract the withdrawal force on the tip, and the MD simulations clearly model transfer of material between opposing asperities under pristine surface conditions. Landman has subsequently conducted numerous other MD simulations, including complete indentation and indentation in the presence of organic species between the indenter and substrate. Belak and Stowers [47], using a material volume containing 43,440 atoms in 160 layers, simulated many of the deformational features associated with metals, such as edge dislocations, plastic zones, and point defect generation. Calculated shear stresses for a triangular indenter passing along the surface exhibited erratic behaviour, not unlike that observed during metallic sliding under clean conditions. Pollock and Singer [48] compiled a series of papers on atomic-scale approaches to friction.

While MD simulations and atomic-scale experiments continue to provide fascinating insights into frictional behaviour, under idealized conditions, most engineering tribosystems are non-uniform. Not only are surfaces not atomically flat, but the materials are not homogeneous, and surface films and contaminant particles of many kinds, much larger than the atomic scale, may influence interfacial behaviour. Static friction coefficients measured experimentally under ambient or contaminated conditions probably will not assume the values obtained in controlled environments. In a series of carefully conducted experiments on the role of adsorbed oxygen and chlorine on the shear strength of metallic junctions [49] showed how, $\mu_{s,}$ can be reduced in the presence of adsorbed gases. On the other hand, static friction coefficients for pure, well-cleaned metal surfaces in the presence of non-reactive gases like He can be relatively high. It is interesting to note that the friction of copper on nickel and the friction of nickel on copper are quite different. This is not an error, but rather a demonstration of the fact that reversing the materials of the sliding specimen and the counterface surface can affect the measured friction,

Table 6.4 Static friction coefficients for clean metals in helium gas at two temperatures

Static friction coefficient		
Material combination	300 K	80 K
Fe (99.9 %) on Fe (99.99 %)	1.09	1.04
Al (99 %) on Al (99 %)	1.62	1.60
Cu (99.95 %) on Cu (99.95 %)	1.76	1.70
Ni (99.95 %) on Ni (99.95 %)	2.11	2.00
Au (99.98 %) on Au (99.98 %)	1.88	1.77
Ni (99.95 %) on Cu (99.95 %)	2.34	2.35
Cu (99.95 %) on Ni (99.95 %)	0.85	0.85
Au (99.98 %) on Al (99 %)	1.42	1.50
Fe (99.9 %) on Cu (99.95 %)	1.99	2.03

Reprinted with permission from Jackson and Morrell [31]

confirming the assertion that friction is a property of the tribosystem and not of the materials in contact. A cryotribometer was used to obtain the data in Table 6.4. The length of time that two solids are in contact can also affect the relative role that adhesion plays in establishing the value of the static friction coefficient. Two distinct possibilities can occur: (a) if the contact becomes contaminated with a lower shear-strength species, the friction will decline; and (b) if the contact is clean and a more tenacious interfacial bond develops, the static friction will tend to increase. Akhmatov [50] demonstrated that by using cleaved rock salt that the formation of surface films over time lowers static friction. The opposite effect has been demonstrated for metals. A first approximation of rising static friction behaviour is given by,

$$\mu_{S(t)} = \mu_{S(t=\infty)} - \left[\mu_{S(t=\infty)} - \mu_{S(t=0)}\right] e^{-ut} \tag{6.19}$$

where, $\mu_s(t)$, is the current value of the static friction coefficient at time t, $\mu_s(t = \infty)$ is the limiting value of the static friction coefficient at long times, $\mu_s(t = 0)$ is the initial static friction coefficient, and u is a rate constant. In contrast to exponential dependence on time, Buckley showed that by using data for tests of single-crystal Au touching Cu-5 % Al alloy that junction growth can cause the adhesive force to increase linearly with time.

When materials are placed in intimate contact, it is not unexpected that the atoms on their surfaces will begin to interact. The degree of this interaction will depend on the contact pressure, temperature, and the degree of chemical reactivity that the species have for each other, hence, static friction can change with the duration of contact. Despite the two opposite dependencies of static friction on time of contact, observations are consistent from a thermodynamic standpoint. Systems tend toward the lowest energetic state. In the case of interfaces, this state can be achieved either by forming bonds between the solids, or by forming bonds with other species (adsorbates and films) in the interface. The former process tends to strengthen the

shear strength of the system, and the latter tends to weaken it. Sikorski [51] reported the results of experiments designed to compare friction coefficients of metals with their coefficients of adhesion (defined as the ratio of the force needed to break the bond between two specimens to the force which initially compressed them together). Rabinowicz [52] conducted a series of simple, tilting-plane tests with milligram- to kilogram-sized specimens of a variety of metals. Results demonstrated the static friction coefficient to increase as slider weight (normal force) decreased. For metal couples such as Au/Rh, Au/Au, Au/Pd, Ag/Ag, and Ag/Au, as the normal force increased over about six orders of magnitude (1 mg–1 kg), the static friction coefficients tended to decrease by nearly one order of magnitude.

Under low contact pressures, surface chemistry effects can play a relatively large role in governing static friction behaviour. However, under more severe contact conditions, such as extreme pressures and high temperatures, other factors, more directly related to bulk properties of the solids, dominate static friction behaviour. When very high pressures and temperatures are applied to solid contacts, diffusion bonds or solid-state welds can form between solids, and the term static friction ceases to be applicable. Table 6.5 lists a series of reported static friction coefficients. Note that in certain cases, the table references list quite different values for these coefficients. The temperature of sliding contact can affect the static friction coefficient. This behaviour was demonstrated for single crystal ceramics by Miyoshi and Buckley [41], who conducted static friction tests of pure iron sliding on cleaned {0001} crystal surfaces of silicon carbide in a vacuum (10^{-8} Pa). For both <1010> and <1120> sliding directions, the static friction coefficients remained about level (0.4 and 0.5, respectively) from room temperature up to about 400 °C; then they each rose by about 50 % as the temperature rose to 800 °C. The authors attributed this effect to increased adhesion and plastic flow. The role of adsorbed films on static friction suggests that one effective strategy for alleviating or reducing static friction is to introduce a lubricant or other surface treatment to impede the formation of adhesive bonds between mating surfaces. Contamination of surfaces from exposure to the ambient environment performs essentially the same function, but is usually less reproducible. Campbell [53] demonstrated how the treatment of metallic surfaces by oxidation can reduce the static friction coefficient. Oxide films were produced by heating metals in air. Sulfide films were produced by immersing the metals in sodium sulfide solution.

Except for the film on steel, film thicknesses were estimated to be 100–200 nm. Results from ten experiments, using a three ball-on-flat plate apparatus, were averaged to obtain static friction coefficients. In addition to producing oxides and sulfides, Campbell also tested oxide and sulfide films with Acto oil. The results of this investigation are shown in Table 6.6. For copper, the static friction coefficient (μ_s = 1.21, with no film) decreased when the sulfide film thickness was increased from 0 to about 300 nm, after which the static friction coefficient remained about constant at 0.66.

The extent to which the solid lubricant can reduce static friction may be dependent on temperature, as confirmed by Hardy's earlier studies on the static friction of palmitic acid films on quartz. Between 20 and 50 °C the static friction

Table 6.5 Static friction coefficients for metals and non-metals (dry or unlubricated conditions)

Material combination			
Fixed specimen	Moving specimen	μ_s	Table reference number
Metals and alloys on various materials			
Aluminium	Aluminium	1.05	1
	Steel, mild	0.61	1
	Titanium	0.54	3
Al, 6061-T6	Al, 6061-T6	0.42	4
	Copper	0.28	4
	Steel, 1032	0.35	4
	Ti-6Al-4 V	0.34	4
Copper	Cast iron	1.05	1
Steel	Cast iron	0.4	2
Steel, hardened	Steel, hardened	0.78	1
	Babbitt	0.42, 0.70	1
	Graphite	0.21	1
Steel, mild	Steel, mild	0.74	1
	Lead	0.95	1
Steel, 1032	Aluminium	0.47	4
	Copper	0.32	4
	Steel, 1032	0.31	4
	Ti-6Al-4 V	0.36	4
Steel, stainless 304	Copper	0.33	4
Tin	Iron	0.55	3
	Tin	0.74	3
Titanium	Aluminium	0.54	3
	Titanium	0.55	3

Reprinted with permission from Jackson and Morrell [31]
1. Bhushan and Gupta [104]
2. Handbook of Chemistry and Physics, 48th Ed., CRC Press (1967)
3. E. Rabinowicz, ASLE Trans., Vol. 14, p. 198; plate sliding on inclined plate at 50 % rel. humidity (1971)
4. "Friction Data Guide," General Magnaplate Corp., Ventura, California 93003, TMI Model 98-5 Slip and Friction Tester, 200 grams load, ground specimens, 54 % rel. humiityd, average of 5 tests (1988)

Table 6.6 Reduction of static friction by surface films

Material combination	μ_s, No film	μ_s, Oxide film	μ_s, Sulfide film
Copper-on-copper	1.21	0.76	0.66
Steel on steel	0.78	0.27	0.39
Steel on steel	078	0.19[a]	0.16[a]

Reprinted with permission from Jackson and Morrell [31]
[a] film and oil

coefficient decreases until melting occurs, at which time the lubricant loses its effectiveness.

Stick-slip is often referred to as a relaxation-oscillation phenomenon, and consequently, some degree of elasticity is needed in the sliding contact in order for stick-slip to occur. Israelachvili [54] considered stick-slip on a molecular level, as measured with surface forces apparatus. He considers the order-disorder transformations described by Thompson and Robbins [44], 1991) in terms of simulations. Most classical treatments of stick-slip take a mechanics approach, considering that the behaviour in unlubricated solid sliding is caused by forming and breaking adhesive bonds.

Stick-slip behaviour can be modeled in several ways. Generally, the system is represented schematically as a spring-loaded contact, sometimes including a dashpot element to account for viscoelastic response [55]. The effects of time-dependent material properties on stick-slip behaviour of metals are provided by Kosterin and Kragelski [56] and Kragelski [57]. Bowden and Tabor's analysis [58] considers a free surface of inertial mass m being driven with a uniform speed ν in the positive x direction against an elastic constant k. Then the instantaneous resisting force **F** over distance x equals—kx. With no damping of the resultant oscillation,

$$ma = -kx \tag{6.20}$$

where acceleration $a = (d^2x/dt^2)$. The frequency n of simple harmonic motion is given by

$$n = (1/2\,\pi)(k/m)^{1/2} \tag{6.21}$$

Under the influence of a load **P** (mass **W** acting downward with the help of gravity g), the static friction force $\mathbf{F}_s$ can be represented as

$$\mathbf{F}_s = \mu_s \mathbf{P} \tag{6.22}$$

In terms of the deflection at the point of slip (x),

$$x = \mathbf{F}_s/k \tag{6.23}$$

If the kinetic friction coefficient μ is assumed to be constant during slip, then

$$ma - \mu\mathbf{P} = -kx \tag{6.24}$$

Letting time = 0 at the point of slip (where $x = F_s/k$), and the forward velocity ν < < the velocity of slip, then,

$$x = (\mathbf{P}/k)[(\mu_s - \mu)\ \cos\ \omega t + \mu] \tag{6.25}$$

where, $\omega = (k/m)$.$^{1/2}$ In this case, the magnitude of slip, δ, is

$$\delta = [\mathbf{P}(2\mu_s - 2\mu)/k] \tag{6.26}$$

From this equation, the larger the μ relative to μ_s, the less the effects of stick-slip, and when they are equal, the sliding becomes completely steady. Kudinov and Tolstoy [59] derived a critical velocity above which stick-slip could be suppressed. This critical velocity v_c was directly proportional to the difference in the static and kinetic friction coefficients Δμ and inversely proportional to the square root of the product of the relative dissipation of energy during oscillation ($\psi = 4\pi\tau$), the stiffness of the system k, and the slider mass m. Thus,

$$v_c = \Delta\mu N/\sqrt{\psi km} \tag{6.27}$$

where N is the factor of safety. The authors report several characteristic values of Δμ for slideways on machine tools: cast iron on cast iron = 0.08, steel on cast iron = 0.05, bronze on cast iron = 0.02, and PTFE on cast iron = 0.04.

System resonance within limited stick-slip oscillation ranges was discussed by Bartenev and Lavrentev [60], who cited experiments in which an oscillating normal load was applied to a system in which stick-slip was occurring. The minimum in stick-slip amplitude and friction force occurred over a range of about 1.5–2.5 kHz, the approximate value predicted by $(1/2\pi)(k/m)^{-1/2}$. Rabinowicz [61] suggested two possible solutions:

1. Decrease the slip amplitude or slip velocity by increasing contact stiffness, increasing system damping, or increasing inertia; and
2. Lubricate or otherwise form a surface film to ensure a positive μ versus velocity relationship.

The latter solution requires that effective lubrication be maintained, and stick-slip can return if the lubricant becomes depleted. The fact that stick-slip is associated with a significant difference between static and kinetic friction coefficients suggest that strategies that lower the former or raise the latter can be equally effective.

6.3.1.2 Sliding Friction

Sliding friction plays a very important role in many manufacturing processes. Sliding friction models, other than empirical models, can generally be grouped into five categories:

1. Ploughing and cutting-based models;
2. Adhesion, junction-growth, and shear models;
3. Single- and multiple-layer shear models;
4. Debris layer and transfer layer models; and
5. Molecular dynamics' models.

Each type of model was developed to explain frictional phenomena. Some of the models are based on observations that contact surfaces contain grooves that are suggestive of a dominant contribution from ploughing. Single-layer models rely on a view of the interface showing flat surfaces separated by a layer whose shear strength controls friction. Some models involve combinations, such as adhesion plus ploughing. Recent friction models contain molecular-level phenomena. Lubrication-oriented models and the debris-based models describe phenomena that take place in zone I, whereas most of the classical models for solid friction concern zone II phenomena. There are few models that take into account the effects of both the interfacial properties and the surrounding mechanical systems such as zone III models.

Models for Sliding Friction

Sliding friction models are summarized in this section of the chapter and fall into one, or more, of the five categories explained in the previous section.

(a) ***Ploughing Models***: Ploughing models assume that the dominant contribution to friction is the energy required to displace material ahead of a rigid protuberance or protuberances moving along a surface. One of the simplest models for ploughing is that of a rigid cone of slant angle θ ploughing through a surface under a normal load **P** [61]. If we assign a groove width w (i.e., twice the radius r of the circular section of the penetrating cone at surface level), the triangular projected area, A_p, swept out as the cone moves along is as follows:

$$A_p = \frac{1}{2} w(r \tan \theta) = \frac{1}{2}(2r)(r \tan \theta) = r^2 \tan \theta \tag{6.28}$$

The friction force $\mathbf{F}_p$ for this ploughing contribution to sliding is found by multiplying the swept-out area by the compressive strength p. Thus, $\mathbf{F}_p = (r^2 \tan \theta)\, p$, and the friction coefficient, if this were the only contribution, is $\mu_p = \mathbf{F}_p/\mathbf{P}$. From the definition of the compressive strength p as force per unit area, we can write:

$$p = \mathbf{P}/\pi r^2 \tag{6.29}$$

And

$$\mu_p = \mathbf{F}_p/\mathbf{P} = \left(r^2 \tan \theta\right) p/\pi r^2 p = (\tan \theta)/\pi \tag{6.30}$$

This expression can also be written in terms of the apex angle of the cone ($\alpha = 90 - \theta$):

Table 6.7 Estimates of the maximum ploughing contribution to friction

Metal	Critical rake angle[a] (°)	μ_p
Aluminium	−5	0.03
Nickel	−5	0.03
Lead	−35	0.22
α-Brass	−35	0.22
Copper	−45	0.32

Reprinted with permission from Jackson and Morrell [31]
[a] For a cone, the absolute value of the critical rake angle is 90 minus angle θ

$$\mu_p = (2 \cot \alpha)/\pi \tag{6.31}$$

Note that the friction coefficient calculated is for the ploughing of a hard asperity and is not necessarily the same as the friction coefficient of the material sliding along the sides of the conical surface. Table 6.7 shows the maximum ploughing contribution to friction for various metals.

(b) ***Adhesion, Junction Growth, and Shear (AJS) Models***: The AJS interpretations of friction are based on a scenario in which two rough surfaces are brought close together, causing the highest peaks (asperities) to touch. As the normal force increases, the contact area increases and the peaks are flattened. Asperity junctions grow until they are able to support the applied load. Adhesive bonds form at the contact points. When a tangential force is applied, the bonds must be broken, and overcoming the shear strength of the bonds results in the friction force. Early calculations comparing bond strengths to friction forces obtained in experiments raised questions as to the general validity of such models. Observations of material transfer and similar phenomena suggested that the adhesive bonds might be stronger than the softer of the two bonded materials, and that the shear strength of the softer material, not the bond strength, should be used in friction models.

Traditional friction models, largely developed for metal-on-metal sliding, have added the force contribution due to the shear of junctions to the contribution from ploughing, giving the extended expression:

$$\mu = (\tau A_r)/\mathbf{P} + (\tan \theta)/\pi \tag{6.32}$$

where A_r is the real area of contact and τ is the shear strength of the material being plowed. This type of expression has met with relatively widespread acceptance in the academic community and is often used as the basis for other sliding friction models. But if the tip of the cone wears down, three contributions to the ploughing process can be identified: the force needed to displace material from in front of the cone, the friction force along the leading face of the cone (i.e., the component in the macroscopic sliding direction), and the friction associated with shear of the interface along the worn frustum of the cone. From this analysis, it is clear that friction

on two scales is involved: the macroscopic friction force for the entire system, and the friction forces associated with the flow of material along the face of the cone and across its frustum. That situation is somewhat analogous to the interpretation of orthogonal cutting of metals in which the friction force of the chip moving up along the rake face of the tool and friction along the wear land are not in general the same as the cutting force for the tool as a whole [62]. Considering the three contributions to the friction of a flat-tipped cone gives

$$\mu = (\tau/\mathbf{P})\left(\pi r^2\right) + \mu_i \cos^2\theta + (\tan\,\theta)/\pi \tag{6.33}$$

where r is defined as the radius of the top of the worn cone and μ_i is the friction coefficient of the cone against the material flowing across its face. Equation 6.33 helps explain why the friction coefficients for ceramics and metals sliding on faceted diamond films are 10 or more times higher than the friction coefficients reported for smooth surfaces of the same materials sliding against smooth surfaces of diamond (i.e., $\mu >> \mu_i$). When the rake angle θ is small, $\cos^2\theta$ is close to 1.0. The second term is only slightly less than μ_i (0.02–0.12 typically). If one assumes that the friction coefficient for the material sliding across the frustum of the cone is the same as that for sliding along its face (μ_i), then Eq. 6.33 can be re-written:

$$\mu = 2\mu_i + (\tan\,\theta)/\pi \tag{6.34}$$

Thus, this implies that the friction coefficient for a rigid sliding cone is more than twice that for sliding a flat surface of the same two materials. It is interesting to note that Eq. 6.34 does not account for the depth of penetration, a factor that seems critical for accounting for the energy required to plow through the surface (displace the volume of material ahead of the slider), and at $\theta = 90^o$, which implies infinitely deep penetration of the cone, it would be impossible to move the slider at all as μ tends toward infinity.

When one of the complexities of surface finish it seems remarkable that Eqs. 6.33 and 6.34, which depend on a single quantity [$(\tan\theta)/\pi$], should be able to predict the friction coefficient with any degree of accuracy. The model is based on a single conical asperity cutting through a surface that makes no obvious accountability for multiple contacts and differences in contact angle. The model is also based on a surface's relatively ductile response to a perfectly rigid asperity and can neither account for fracture during wear nor account for the change in the groove geometry that one would expect for multiple passes over the same surface.

Mulhearn and Samuels [63] published a paper on the transition between abrasive asperities cutting through a surface and ploughing through it. The results of their experiments suggested that there exists a critical rake angle for that type of transition. (Note: The rake angle is the angle between the normal to the surface and the leading face of the asperity, with negative values indicating a tilt toward the direction of travel). If ploughing can occur only up to the critical rake angle, then we may compute the maximum contribution to friction due to ploughing from the data of Mulhearn and Samuels and Eq. 6.31 (Table 6.7). This approach suggests

Table 6.8 Critical degree of penetration (D_p) for unlubricated friction mode transitions

	Value of D_p for the transition	
Material	Ploughing to wedge formation	Wedge formation to cutting
Brass	0.17 (tip radius 62 μm)	0.23 (tip radius 62, 27 μm)
Carbon steel	0.12 (tip radius 62 μm)	0.23 (tip radius 27 μm)
Stainless steel	0.13 (tip radius 62, 27 μm)	0.26 (tip radius 27 μm)

Reprinted with permission from Jackson and Morrell [31]

that the maximum contribution of ploughing to the friction coefficient of aluminium or nickel is about 0.03 in contrast to copper, whose maximum ploughing contribution is 0.32. Since the sliding friction coefficient for aluminium can be quite high (over 1.0 in some cases), the implication is that factors other than ploughing, such as the shearing of strongly adhering junctions, would be the major contributor. Examination of unlubricated sliding wear surfaces of both Al and Cu often reveals a host of ductile-appearing features not in any way resembling cones, and despite the similar appearances in the microscope of worn Cu and Al, one finds from the first and last rows in Table 6.8 that the contribution of ploughing to friction should be different by a factor of 10. Again, the simple cone model appears to be too simple to account for the difference.

Hokkirigawa and Kato [64] carried the analysis of abrasive contributions to sliding friction even further using observations of single hemispherical sliding contacts (quenched steel, tip radius 26 or 62 μm) on brass, carbon steel, and stainless steel in a scanning electron microscope. They identified three modes: (a) ploughing, (b) wedge formation and (c) cutting (chip formation). The tendency of the slider to produce the various modes was related to the degree of penetration, D_p. Here, D_p. Here, $D_p = h/a$, where h is the groove depth and a is the radius of the sliding contact. The sliding friction coefficient was modeled in three ways depending upon the regime of sliding. Three parameters were introduced:

$$f = p/\tau \qquad \theta = \sin^{-1}(a/R)$$

and β, the angle of the stress discontinuity (shear zone) from Challen and Oxley's [65] analysis. Where p is the contact pressure, τ is the bulk shear stress of the flat specimen, and R is the slider tip radius. The friction coefficient was given as follows for each mode:

Cutting mode:

$$\mu = \tan\left[\theta - (\pi/4) + \frac{1}{2}\cos^{-1} f\right] \tag{6.35}$$

Wedge-forming mode:

$$\mu = \frac{\left\{1 - \sin 2\beta + (1 - f^2)^{1/2}\right\} \sin\theta + f\cos\theta}{\left\{1 - \sin 2\beta + (1 - f^2)^{1/2}\right\} \cos\theta + f\sin\theta} \tag{6.36}$$

Ploughing mode:

$$\mu = \frac{A\sin\theta + \cos(\cos^{-1} f - \theta)}{A\sin\theta + \cos(\cos^{-1} f - \theta)} \tag{6.37}$$

where

$$A = 1 + (\pi/2) + \cos^{-1} f - 2\theta - 2\sin^{-1}\frac{\sin\theta}{(1-f)^{-1/2}} \tag{6.38}$$

For unlubricated conditions, the transitions between the various modes were experimentally determined by observation in the scanning electron microscope. Table 6.8 summarizes those results. Results of the study illustrate the point that the analytical form of the frictional dependence on the shape of asperities cannot ignore the mode of surface deformation. In summary, the foregoing treatments of the ploughing contribution to friction assumed that asperities could be modeled as regular geometric shapes. However, rarely do such shapes appear on actual sliding surfaces. The asperities present on most sliding surfaces are irregular in shape, as viewed with a scanning electron microscope.

(c) ***Ploughing with Debris Generation***: Even when the predominant contribution to friction is initially from cutting and ploughing of hard asperities through the surface, the generation of wear debris that submerges the asperities can reduce the severity of ploughing. Table 6.9 shows that starting with multiple hard asperities of the same geometric characteristics produced different initial and steady-state friction coefficients for the three slider materials. Wear debris accumulation in the contact region affected the frictional behaviour. In the case of abrasive papers and grinding wheels, this is called loading. Loading is extremely important in grinding, and a great deal of effort has been focused on dressing grinding wheels to improve their material removal efficiency. One measure of the need for grinding wheel dressing is an increase in the tangential grinding force or an increase in the power drawn by the grinding spindle.

As wear progresses, the wear debris accumulates between the asperities and alters the effectiveness of the cutting and ploughing action by covering the active points. If the cone model is to be useful at all for other than pristine surfaces, the effective value of θ must be given as a function of time or number of sliding passes. Not only is the wear rate affected, but the presence of debris affects the interfacial shear strength, as is explained later in this chapter in regard to third-body particle

Table 6.9 Effects of material type on friction during abrasive sliding

	24 μm grit size		16 μm grit size	
Slider material	Starting (μ)	Ending (μ)	Starting (μ)	Ending (μ)
AISI 52100 steel	0.47	0.35	0.45	0.29
2014-T4 aluminium	0.69	0.56	0.64	0.62
PMMA	0.73	0.64	0.72	0.60

Reprinted with permission from Jackson and Morrell [31]
[a] Normal force 2.49 N, sliding speed 5 mm/s, multiple strokes 20 mm long

effects on friction. The observation that wear debris can accumulate and so affect friction has led investigators to try patterning surfaces to create pockets where debris can be collected [66]. The orientation and depths of the ridges and grooves in a surface affect the effectiveness of the debris-trapping mechanism.

(d) ***Ploughing with Adhesion***: Traditional models for sliding friction have historically been developed with metallic materials in mind. Classically, the friction force is said to be an additive contribution of adhesive (S) and ploughing forces ($\mathbf{F}_{\text{pl}}$) [58]:

$$\mathbf{F} = \mathbf{S} + \mathbf{F}_{\text{pl}} \tag{6.39}$$

The adhesive force derives from the shear strength of adhesive metallic junctions that are created when surfaces touch one another under a normal force. Thus, by dividing by the normal force we find that $\mu = \mu_{\text{adhesion}} + \mu_{\text{ploughing}}$. If the shear strength of the junction is τ and the contact area is A, then

$$\mathbf{S} = \tau A \tag{6.40}$$

The ploughing force $\mathbf{F}_{\text{pl}}$ is given by

$$\mathbf{F}_{\text{pl}} = pA' \tag{6.41}$$

where p is the mean pressure to displace the metal in the surface and A' is the cross section of the grooved wear track. While helpful in understanding the results of experiments in the sliding friction of metals, the approach involves several applicability-limiting assumptions, for example, that adhesion between the surfaces results in bonds that are continually forming and breaking, that the protuberances of the harder of the two contacting surfaces remain perfectly rigid as they plow through the softer counterface, and perhaps most limiting of all, that the friction coefficient for a tribosystem is determined only from the shear strength properties of materials.

(e) ***Single-Layer Shear* (*SLS*) *Models***: SLS models for friction depict an interface as a layer whose shear strength determines the friction force, and hence, the friction coefficient. The layer can be a separate film, like a solid lubricant, or simply the near surface zone of the softer material that is shearing during friction. The friction force **F** is the product of the contact area A and the shear strength of the layer:

$$\mathbf{F}=\tau A \tag{6.42}$$

The concept that the friction force is linearly related to the shear strength of the interfacial material has a number of useful implications, especially as regards the role of thin lubricating layers, including oxides and tarnish films. It is known from the work of Bridgman [67] on the effects of pressure on mechanical properties that τ is affected by contact pressure, p:

$$\tau = \tau_o + \alpha p \tag{6.43}$$

Table 6.10 lists several values for the shear stress and the constant α [68].

(f) ***Multiple-Layer Shear* (*MLS*) *Models***: SLS models presume that the sliding friction can be explained on the basis of the shear strength on a single layer interposed between solid surfaces. Evidence revealed by the examination of frictional surfaces suggests that shear can occur at various positions in the interface: for example, at the upper interface between the solid and the debris layer, within the entrapped debris or transfer layer itself, at the lower interface, or even below the original surfaces where extended delaminations may occur. Therefore, one may construct a picture of sliding friction that involves a series of shear layers (sliding resistances) in parallel. Certainly, one would expect the predominant frictional contribution to be the lowest shear strength in the shear

Table 6.10 Measured values for the shear stress dependence on pressure

Material	τ_o (kgf/mm^2)	α
Aluminium	3.00	0.043
Beryllium	0.45	0.250
Chromium	5.00	0.240
Copper	1.00	0.110
Lead	0.90	0.014
Platinum	9.50	0.100
Silver	6.50	0.090
Tin	1.25	0.012
Vanadium	1.80	0.250
Zinc	8.00	0.020

Reprinted with permission from Jackson and Morrell [31]

layers. Yet the shear forces transmitted across the weakest interface may still be sufficient to permit some displacement to occur at one or more of the other layers above or below it, particularly if the difference in shear strengths between those layers is small.

The MLS models can be treated like electrical resistances in a series. The overall resistance of such a circuit is less than any of the individual resistances because multiple current paths exist. Consider, for example, the case where there are three possible operable shear planes stacked up parallel to the sliding direction in the interface. Then,

$$\frac{1}{\mathbf{F}}=\frac{1}{\mathbf{F}_1}+\frac{1}{\mathbf{F}_2}+\frac{1}{\mathbf{F}_3} \tag{6.44}$$

And, solving for the total friction force **F**, in terms of the friction forces acting on the three layers, is

$$\mathbf{F}=\frac{\mathbf{F}_1\mathbf{F}_2\mathbf{F}_3}{\mathbf{F}_1\mathbf{F}_2+\mathbf{F}_2\mathbf{F}_3+\mathbf{F}_1\mathbf{F}_3} \tag{6.45}$$

If the area of contact *A* is the same across each layer, then Eq. 6.45 can be written in terms of the friction coefficient of the interface, the shear stresses of each layer, and the normal load **P** as follows:

$$\mu=\left(\frac{\mathrm{A}}{\mathbf{P}}\right)\left[\frac{\tau_1\,\tau_2\,\tau_3}{\tau_1\,\tau_2+\tau_2\,\tau_3+\tau_1\,\tau_3}\right] \tag{6.46}$$

If one of the shear planes suddenly became unable to deform (say, by work hardening or by clogging with a compressed clump of wear debris), the location of the governing plane of shear may shift quickly, causing the friction to fluctuate. Thus, by writing the shear stresses of each layer as functions of time, the MLS model has the advantage of being able to account for variations in friction force with time and may account for some of the features observed in microscopic examinations of wear tracks.

(g) ***Molecular Dynamics' Models***: When coupled with information from nanoprobe instruments, such as the atomic force microscope, the scanning tunneling microscope, the surface-forces apparatus, and the lateral-force microscope, MD studies have made possible insights into the behaviour of pristine surfaces on the atomic scale. Molecular dynamics models of friction for assemblages of even a few hundred atoms tend to require millions upon millions of individual, iterative computations to predict frictional interactions taking place over only a fraction of a second in real time, because they begin with very specific arrangements of atoms, usually in single crystal form with a

specific sliding orientation, results are often periodic with sliding distance. Some of the calculation results are remarkably similar to certain types of behaviour observed in real materials, simulating such phenomena as dislocations (localized slip on preferred planes) and the adhesive transfer of material to the opposing counterface. However, molecular dynamics models are not presently capable of handling such contact surface features as surface fatigue-induced delaminations, wear debris particles compacting and deforming in the interface, high-strain-rate phenomena, work hardening of near-surface layers, and effects of inclusions and other artifacts present in the microstructures of commercial engineering materials.

The models presented up to this point use either interfacial geometric parameters or materials properties (i.e., bonding energies, shear strengths, or other mechanical properties) to predict friction. Clearly, frictional heating and the chemical environment may affect some of the variables used in these models. For example, the shear strength of many metals decreases as the temperature increases and increases as the speed of deformation increases. Certainly, wear and its consequences (debris) will affect friction. Thus, any of the previously described models will probably require some sort of modification, depending on the actual conditions of sliding contact. In general, the following can be said about friction models:

1. No existing friction model explicitly accounts for all the possible factors that can affect friction;
2. Even very simple friction models may work to some degree under well-defined, limited ranges of conditions, but their applicability must be tested in specific cases;
3. Accurately predictive, comprehensive tribosystem-level models that account for interface geometry, materials properties, lubrication aspects, thermal, chemical, and external mechanical system response, all in a time-dependent context, do not exist;
4. Friction models should be selected and used based on an understanding of their limitations and on as complete as possible an understanding of the dominant influences in the tribosystem to which the models will be applied; and
5. Current quantitative models produce a single value for the friction force, or friction coefficient. Since the friction force in nearly all known tribosystems varies to some degree, any model that predicts a single value is questionable.

If no existing model is deemed appropriate, the investigator could either modify a current model to account for the additional variables, develop a new system-specific model, or revert to simulative testing and/or field experiments to obtain the approximate value. An alternative to modeling is to estimate frictional behaviour using a graphical, or statistical approach.

6.3.2 Frictional Heating

Heat generation and rising surface temperatures are intuitively associated with friction. When a friction force **F** moves through a distance x, an amount of energy $\mathbf{F}x$ is produced. The laws of thermodynamics require that the energy so produced be dissipated to the surroundings. At equilibrium, the energy into a system $\mathbf{U}_{in}$ equals the sum of the energy output to the surroundings $\mathbf{U}_{out}$ (dissipated externally) and the energy accumulated $\mathbf{U}_{accumulated}$ (consumed or stored internally):

$$U_{in} = U_{out} + U_{accumulated} \tag{6.47}$$

The rate of energy input in friction is the product of **F** and the sliding velocity v whose units work out to energy per unit time (e.g., Nm/s). This energy input rate at the frictional interface is balanced almost completely by heat conduction away from the interface, either into the contacting solids or by radiation or convection to the surroundings. In general, only a small amount of frictional energy, perhaps only 5 %, is consumed or stored in the material as microstructural defects such as dislocations, the energy to produce phase transformations, surface energy of new wear particles and propagating subsurface cracks, etc. Most of the frictional energy is dissipated as heat. Under certain conditions, there is enough heat to melt the sliding interface. Energy that cannot readily be conducted away from the interface raises the temperature locally. Assuming that the proportionality of friction force **F** to normal force **P** (i.e., by definition, $\mathbf{F} = \mu\mathbf{P}$) holds over a range of normal forces, we would expect that the temperature rise in a constant-velocity sliding system should increase linearly with the normal force. Tribologists distinguish between two temperatures, the flash temperature and the mean surface temperature. The former is localized, the latter averaged out over the nominal contact zone. Since sliding surfaces touch at only a few locations at any instant, the energy is concentrated there and the heating is particularly intense—thus, the name flash temperature. The combined effect of many such flashes dissipating their energy in the interface under steady state is to heat a near-surface layer to an average temperature that is determined by the energy transport conditions embodied in Eq. 6.47 given earlier. Blok [69] discussed the concept and calculation of flash temperature in a review article. The early work of Blok [70] and Jaeger [71] is still cited as a basis for more recent work, and it has been reviewed in a simplified form by Bowden and Tabor [58]. Basically, the temperature rise in the interface is given as a function of the total heat developed, Q:

$$Q = \frac{\mu \mathbf{W} g v}{J} \tag{6.48}$$

where, μ is the sliding friction coefficient, **W** is the load, g the acceleration due to gravity, v the sliding velocity, and J the mechanical equivalent of heat (4.186 J/cal). Expressions for various heat flow conditions are then developed based on Eq. 6.48. Some of these are given in Table 6.11.

Table 6.11 Temperature rise during sliding

Conditions	Temperature rise[a] ($T = T_o$)
Circular junction of radius a	$= \frac{Q}{4a(k_1+k_2)}$
Square junction of side = 2 l, at low speed	$= \frac{Q}{4.24l(k_1+k_2)}$
Square junction of side = 2 l, at high speed wherein the slider is being cooled by the incoming surface of the flat disk specimen	$= \frac{Q\mathrm{x}^{1/2}}{3.76l\left[k_1(l/\mathrm{v})^{1/2}+1.125\mathrm{x}^{1/2}k_2\right]}$
	Where $\mathrm{x} = (k_1/\rho_1 c_1)$ for the disk material

After Jaeger [71]. Reprinted with permission from Jackson and Morrell [31]
[a] T = steady-state junction temperature, T_o = initial temperature, $k_{1,2}$ = thermal conductivity of the slider and flat bodies, ρ = density, c = specific heat

As Table 6.11 shows, the expressions become more complicated when the cooling effects of the incoming, cooler surface are accounted for. Rabinowicz [61] published an expression for estimating the flash temperature rise in sliding:

$$\theta_m = \frac{v}{2} (\pm \text{ a factor of 2 to 3}) \tag{6.49}$$

where, v is sliding velocity (ft/min) and θ_m is the estimated surface flash temperature (°F). A comparison of the results of using Eq. 6.49 with several other, more complicated models for frictional heating has provided similar results, but more rigorous treatments are sometimes required to account for the variables left out of this rule of thumb. In general, nearly all models for flash or mean temperature rise during sliding contain the friction force-velocity product. Sometimes, the friction force is written as the product of the normal force and friction coefficients.

A review of frictional heating calculations has been provided by Cowan and Winer [72], along with representative materials properties data to be used in those calculations. Their approach involves the use of two heat partition coefficients (γ_1 and γ_2) that describe the relative fractions of the total heat that go into each of the contacting bodies, such that $\gamma_1 + \gamma_2 = 1$. The time that a surface is exposed to frictional heating will obviously affect the amount of heat it receives. The Fourier modulus, F_o, a dimensionless parameter, is introduced to establish whether or not steady-state conditions have been reached at each surface. For a contact radius a, an exposure time t, and a thermal diffusivity for body i of D_i,

$$F_o = \frac{D_i t}{a^2} \tag{6.50}$$

The Fourier modulus is taken to be 100 for a surface at steady state conditions. Another useful parameter grouping is the Peclet number P_e, defined in terms of the density of the solid ρ, the specific heat c_p, the sliding velocity v, the thermal conductivity k, and the characteristic length L_c:

$$P_e = \frac{\rho c_p v L_c}{k} \tag{6.51}$$

The characteristic length is the contact width for a line contact or the contact radius for a circular contact. The Peclet number relates the thermal energy removed by the surrounding medium to that conducted away from the region in which frictional energy is being dissipated. As $D_i = (\rho c_p/k)$ yields the following,

$$P_e = \frac{v L_c}{D_i} \tag{6.52}$$

The Peclet number is sometimes used as a criterion for determining when to apply various forms of frictional heating models. Peclet number is used in understanding frictional heating problems associated with grinding and machining processes. It is important to compare the forms of models derived by different authors for calculating flash temperature rise. Four treatments for a pin moving along a stationary flat specimen are briefly compared: Rabinowicz's derivation based on surface energy considerations, a single case from Cowan and Winer's review, Kuhlmann-Wilsdorf's model, and the model provided by Ashby. Based on considerations of junctions of radius r and surface energy of the softer material Γ, Rabinowicz arrived at the following expression:

$$T_f = \frac{3000\,\pi\mu\Gamma v}{J(k_1 + k_2)} \tag{6.53}$$

where J is the mechanical equivalent of heat, v is sliding velocity, μ is the friction coefficient, and k_1 and k_2 represent the thermal conductivities of the two bodies. The constant 3,000 obtained from the calculation of the effective contact radius r in terms of the surface energy of the circular junctions Γ and their hardness H (i.e., r = 12,000 ΓH) and the load carried by each asperity ($\mathbf{P} = \pi r^2 H$). Thus, the numerator is actually the equivalent of $\mathbf{F}v$ expressed in terms of the surface energy model. The equation provided by Cowan and Winer, for the case of a circular contact with one body in motion is

$$T_f = \frac{\gamma_1 \mu \mathbf{P} v}{\pi a k_1} \tag{6.54}$$

where γ_1 is the heat partition coefficient, described earlier, $\mathbf{P}$ is the normal force, a is the radius of contact, and k_1 is as defined earlier. The value of γ_1 takes various forms depending on the specific case. The presence of elastic, or plastic contact, can also affect the form of the average flash temperature, as Table 6.12 demonstrates. Here, the exponents of normal force and velocity are not unity in all cases. Kuhlmann-Wilsdorf [73] considered an elliptical contact area as the planar moving heat source. The flash temperature is given in terms of the average temperature in the interface T_{ave}:

Table 6.12 Effects of deformation type and Peclet number on flash temperature calculation for the circular contact case

Type of deformation	Peclet number	Average flash temperature[a]
Plastic	$P_e < 0.02$	$T_f = \mu \mathbf{P}^{0.5} \mathrm{v} \frac{\sqrt{\pi \rho}}{8k}$
Plastic	$P_e > 200$	$T_f = 0.31\,\mu\,\mathbf{P}^{0.25} \mathrm{v}^{0.5} \left[\frac{(\pi \rho)^{0.75}}{(k\,\rho\,C)^{0.5}}\right]$
Elastic	$P_e < 0.02$	$T_f = 0.13 \mu\, \mathbf{P}^{0.667} \mathrm{v} \left(\frac{1}{k}\right) \left(\frac{E_v}{R}\right)^{0.333}$
Elastic	$P_e > 200$	$T_f = 0.36 \mu\, \mathbf{P}^{0.5} v^{0.5} \left(\frac{1}{\sqrt{k \rho c}}\right) \left(\frac{E_v}{R}\right)^{0.5}$

Reprinted with permission from Jackson and Morrell [31]

[a] *Key* μ = friction coefficient, **P** = load, v = velocity, k = thermal conductivity, π = density, c = heat capacity, E_v = the reduced elastic modulus = $E/(1 - \mathrm{v}^2)$, v = Poisson's ratio, ρ = flow pressure of the softer material

$$T_{\mathrm{ave}} = \frac{\pi\, qr}{4k_1} \tag{6.55}$$

where q is the rate of heat input per unit area (related to the product of friction force and velocity), r is the contact spot radius, and k_1 is the thermal conductivity, as given earlier. Then

$$T_{\mathrm{f}} = \frac{T_{\mathrm{avc}}}{(1/ZS) + (k_1/S_{\mathrm{O}})} \tag{6.56}$$

where Z is a velocity function and S and S_o are contact area shape functions (both = 1.0 for circular contact). At low speeds, where the relative velocity of the surfaces $v_r < 2(v_r = v/\mathbf{P}_e)$, Z can be approximated by $1/[1 + (v_r/3)]$. The differences between models for frictional heating arise from the following:

1. Assuming different shapes for the heat source on the surface;
2. Different ways to partition the flow (dissipation) of heat between sliding bodies;
3. Different ways to account for thermal properties of materials (e.g., using thermal diffusivity instead of thermal conductivity, etc.);
4. Different contact geometry (sphere-on-plane, flat-on-flat, cylinder-on-flat, etc.);
5. Assuming heat is produced from a layer (volume) instead of a planar area; and
6. Changes in the form of the expression as the sliding velocity increases.

Comparing the temperature rises predicted by different models for low sliding speeds produces accurate results, even with the uncertainties in the values of the material properties that go into the calculations. At higher speeds, the predictions become unreliable since materials properties change as a function of temperature and the likelihood of the interface reaching a steady state is much lower. Experimental studies have provided very useful information in validating the forms of frictional heating models. Experimental scientists have often used embedded thermocouples in one or both members of the sliding contact to measure surface

temperatures, and others sometimes made thermocouples out of the contacts themselves. However, techniques using infrared sensors have been used as well. Dow and Stockwell [74] used infrared detectors with a thin, transparent sapphire blade sliding on a 15-cm-diameter ground cylindrical drum to study the movements and temperatures of hot spots. Griffioen et al. [75] and Quinn and Winer [76] used an infrared technique with a sphere-on-transparent sapphire disk geometry. A similar arrangement was also developed and used by Furey with copper, iron, and silver spheres sliding on sapphire, and Enthoven et al. [77] used an infrared system with a ball-on-flat arrangement to study the relationship between scuffing and the critical temperature for its onset.

Frictional heating is important because it changes the shear strengths of the materials in the sliding contact, promotes reactions of the sliding surfaces with chemical species in the environment, enhances diffusion of species, and can result in the breakdown or failure of the lubricant to perform its functions. Under extreme conditions, such as plastic extrusion, frictional heating can result in molten layer formation that serves as a liquid lubricant.

6.3.3 Lubrication to Control Friction in Machining

The frictional characteristics of liquid and solid lubricants and their interaction with materials are reviewed. Comprehensive discussions of the mechanical and chemical engineering aspects of lubrication are available in the literature [78]. The following section was originally published by Jackson and Morrell [31] and appears hereafter.

6.3.3.1 Liquid Lubrication

The process of lubrication is one of supporting the contact pressure between opposing surfaces, helping to separate them, and at the same time reducing the sliding or rolling resistance in the interface. There are several ways to accomplish this. One way is to create in the gap between the bodies geometric conditions that produce a fluid pressure sufficient to prevent the opposing asperities from touching while still permitting shear to be fully accommodated within the fluid. That method relies on fluid mechanics and modifications of the lubricant chemistry to tailor the liquid's properties. Another way to create favorable lubrication conditions is to formulate the liquid lubricant in such a way that chemical species within it react with the surface of the bodies to form shearable solid films. Surface species need not react with the lubricant, but catalyze the reactions that produce these protective films.

Several attributes of liquids make them either suitable or unsuitable as lubricants. Klaus and Tewksbury [79] have discussed these characteristics in some detail. They include:

1. Density;
2. Bulk modulus;
3. Gas solubility;
4. Foaming and air entrainment tendencies;
5. Viscosity and its relationships to temperature and pressure;
6. Vapour pressure;
7. Thermal properties and stability; and
8. Oxidation stability.

The viscosity of fluids usually decreases with temperature and therefore can reduce the usefulness of a lubricant as temperature rises. The term viscosity index, abbreviated VI, is a means to express this variation. The higher the VI, the less the change in viscosity with temperature. One of the types of additives used to reduce the sensitivity of lubricant viscosity to temperature changes is called a VI improver. ASTM test method D 2270 is one procedure used to calculate the VI. The process is described step-by-step in the article by Klaus and Tewksbury [79]. The method involves references to two test oils, the use of two different methods of calculation (depending on the magnitude of VI), and relies on charts and tables.

ASTM Standard D341 recommends using the Walther equation to represent the dependence of lubricant viscosity on temperature. Defining Z as the viscosity in cSt plus a constant (typically ranging from 0.6 to 0.8 with ASTM specifying 0.7), T equal to the temperature in Kelvin or Rankin, and A and B being constants for a given oil, then

$$\log_{10}(\log_{10} Z) = A + B(\log_{10} T) \tag{6.57}$$

Sanchez-Rubio et al. [80] have suggested an alternative method in which the Walther equation is used. In this case, they define a viscosity number (VN) as follows:

$$\mathrm{VN} = \left[1 + \frac{(3.55 + \mathrm{B})}{3.55}\right] \times 100 \tag{6.58}$$

The value of 3.55 was selected because lubricating oils with a VI of 100 have a value of B about equal to −3.55. Using this expression implies that VN = 200 would correspond to an idealized oil whose viscosity has no dependence of viscosity on temperature (i.e., B = 0). The pressure to which oil is subjected can influence its viscosity. The relationship between dynamic viscosity and hydrostatic pressure p can be represented by

$$\eta = \eta_o \exp(\alpha p) \tag{6.59}$$

where η and α vary with the type of oil. Table 6.13 illustrates the wide range of viscosities possible for several liquid lubricants under various temperatures and pressures. The viscosity indices for these oils range from −132 to 195. Viscosity

Table 6.13 Effects of temperature and pressure on viscosity of selected lubricants having various viscosity indexes (All fluids have viscosities of 20 cSt at 40 °C and 0.1 MPa pressure)

Quantity	Fluorolube	Hydrocarbon	Ester	Silicone
Viscosity index	−132	100	151	195
Viscosity (cSt) at −40 °C	500,000	14,000	3600	150
Viscosity (cSt) at −100 °C	2.9	3.9	4.4	9.5
Viscosity (cSt) at −40 °C and 138 MPa	2700	340	110	160
Viscosity (cSt) at −40 °C and 552 MPa	>1,000,000	270,000	4900	48,000

Reprinted with permission from Jackson and Morrell [31]

has a large effect on determining the regime of lubrication and the resultant friction coefficient. Similarly to the effect of strain rate on the shear strength of certain metals, like aluminium, the rate of shear in the fluid can also alter the viscosity of a lubricant.

Ramesh and Clifton [81] constructed a plate impact device to study the shear strength of lubricants at strain rates as high as 900,000/s and found significant effects of shear rate on the critical shear stress of lubricants. In a Newtonian fluid, the ratio of shear stress to shear strain does not vary with stress, but there are other cases, such as for greases and solid dispersions in liquids, where the viscosity varies with the rate of shear. Such fluids are termed non-Newtonian and the standard methods for measuring viscosity cannot be used.

Lubrication regimes determine the effectiveness of fluid film formation, and hence, surface separation. In the first decade of the twentieth century, Stribeck developed a systematic method to understand and depict regimes of journal bearing lubrication, linking the properties of lubricant viscosity (η), rotational velocity of a journal (ω), and contact pressure (p) with the coefficient of friction. Based on the work of Mersey, McKee, and others, the dimension-less group of parameters has evolved into the more recent notation (ZN/p), where Z is viscosity, N is rotational speed, and p is pressure. The Stribeck curve has been widely used in the design of bearings and to explain various types of behaviour in the field of lubrication. At high pressures, or when the lubricant viscosity and/or speed are very low, surfaces may touch, leading to high friction. In that case, friction coefficients are typically in the range of 0.5–2.0. The level plateau at the left of the curve represents the boundary lubrication regime in which friction is lower than for unlubricated sliding contact ($\mu = 0.05$ to about 0.15). The drop-off in friction is called the mixed film regime. The mixed regime refers to a combination of boundary lubrication with hydrodynamic or elastohydrodynamic lubrication. Beyond the minimum in the curve, hydrodynamic and elastohydrodynamic lubrication regimes are said to occur. Friction coefficients under such conditions can be very low. Typical friction coefficients for various types of rolling element bearings range between 0.001 and 0.0018.

The conditions under which a journal bearing of length L, diameter D, and radial clearance C (bore radius minus bearing shaft radius) operates in the hydrodynamic regime can be summarized using a dimensionless parameter known as the Sommerfeld number S, defined by

$$S = \frac{\eta NLD}{P}\left(\frac{\mathrm{R}}{\mathrm{C}}\right)^2 \tag{6.60}$$

where P is the load on the bearing perpendicular to the axis of rotation, N is the rotational speed, η is the dynamic viscosity of the lubricant, and R is the radius of the bore. The more concentrically the bearing operates, the higher the value of S, but as S approaches 0, the lubrication may fail, leading to high friction. Sometimes Stribeck curves are plotted using S instead of (ZN/p) as the abscissa. Raimondi [82] added leakage considerations when they developed design charts in which the logarithm of the Sommerfeld number is plotted against the logarithm of either the friction coefficient or the dimensionless film thickness.

Using small journal bearings, McKee developed the following expression for the coefficient of friction μ based on the journal diameter D, the diametral clearance C, and an experimental variable k, which varies with the length to diameter ratio (L/D) of the bearing [83]:

$$\mu = \left(4.73 \times 10^{-8}\right)\left(\frac{ZN}{p}\right)\left(\frac{D}{C}\right) + k \tag{6.61}$$

The value of k is about 0.015 at $(L/D) = 0.2$, drops rapidly to a minimum of about 0.0013 at $(L/D) = 1.0$, and rises nearly linearly to about 0.0035 at $(L/D) = 3.0$. A simpler expression, discussed by Hutchings [84], can be used for bearings that have no significant eccentricity:

$$\mu = \frac{2\pi}{S}\frac{h}{R} \tag{6.62}$$

where S is the Sommerfeld number, h is the mean film thickness, and R is the journal radius. With good hydrodynamic lubrication and good bearing design, μ can be as low as 0.001.

Hydrodynamic lubrication, sometimes called thick-film lubrication, generally depends on the development of a converging wedge of lubricant in the inlet of the interface. This wedge generates a pressure profile to force the surfaces apart. When the elastic deformation of the solid bodies is similar in extent to the thickness of the lubricant film, then elastohydrodynamic lubrication is said to occur. This latter regime is common in rolling element bearings and gears where high Hertz contact stresses occur. If the contact pressure exceeds the elastic limit of the surfaces, plastic deformation and increasing friction occur. One way to understand and control the various lubrication regimes is by using the specific film thickness (also

called the lambda ratio), defined as the ratio of the minimum film thickness in the interface (h) to the composite root-mean-square (rms) surface roughness σ*:

$$\wedge = h/\sigma* \tag{6.63}$$

where the composite surface roughness is defined in terms of the rms roughness ($\sigma_{1,2}$) of surfaces 1 and 2, respectively:

$$\sigma* = \sqrt{\left(\sigma_1^2 + \sigma_2^2\right)} \tag{6.64}$$

For the boundary regime, $\Lambda << 1$. For the mixed regime $1 < \Lambda < 3$. For the hydrodynamic regime, $\Lambda >> 6$, and for the elastohydrodynamic regime, $3 < \Lambda < 10$. Boundary lubrication produces friction coefficients that are lower than those for unlubricated sliding but higher than those for effective hydrodynamic lubrication, typically in the range $0.05 < \mu < 0.2$. Briscoe and Stolarski [85] have reviewed friction under boundary-lubricated conditions. They cited the earlier work of Bowden, which gave the following expression for the friction coefficient under conditions of boundary lubrication:

$$\mu = \beta\mu_a + (1 - \beta)\mu_1 \tag{6.65}$$

where the adhesive component μ_a and the viscous component of friction μ_1 are given in terms of the shear stress of the adhesive junctions in the solid (metal) τ_m and the shear strength of the boundary film τ_1 under the influence of a contact pressure σ_p:

$$\mu_a = \frac{\tau_m}{\sigma_p} \tag{6.66}$$

The parameter, β, is called the fractional film defect [85] and is:

$$\beta = 1 - \exp\left\{ - \left[\frac{\left(300.9 \times 10^5\right) T_m^{1/2}}{VM^{1/2}} \right] \exp\left(- \frac{E_c}{RT} \right) \right\} \tag{6.67}$$

where M is the molecular weight of the lubricant, V is the sliding velocity, T_m is the melting temperature of the lubricant, E_c is the energy to desorb the lubricant molecules, R is the universal gas constant, and T is the absolute temperature. Various graphical methods have been developed to help select boundary lubricants and to help simplify the task of bearing designers. These methods are based on the design parameters of bearing stress (or normal load) and velocity. One method, developed by Glaeser and Dufrane [86] involves the use of design charts for different bearing materials. An alternate but similar approach was used in developing the so-called IRG transitions diagrams (subsequently abbreviated ITDs), an approach that evolved in the early 1980s, was applied to various bearing steels, and

is still being used to define the conditions under which boundary-lubricated tribosystems operate effectively. Instead of pressure, load is plotted on the ordinate. Three regions of ITDs are defined in terms of their frictional behaviour: Region I, in which the friction trace is relatively low and smooth, Region II, in which the friction trace begins with a high level then settles down to a lower, smoother level, and Region III, in which the friction trace is irregular and remains high. The transitions between Regions I and II or between Regions I and III are described as a collapse of liquid film lubrication. The locations of these transition boundaries for steels were seen to depend more on the surface roughness of the materials and the composition of the lubricants and less on microstructure and composition of the alloys. Any of the following testing geometries can be used to develop ITDs: four-ball machines, ball-on-cylinder machines, crossed-cylinders machines, and flat-on-flat testing machines (including flat-ended pin-on-disk). One important aspect of the use of liquid lubricants is how they are applied, filtered, circulated, and replenished. Lubricants can also be formed on surfaces by the chemical reaction of vapour-phase precursor species in argon and nitrogen environments".

6.4 Analysis of Gaps in the Literature and Their Relationship to Grinding Process Interactions

This section allows the reader to identify and understand the gaps in the research literature that pertains to the application of tribological theories to the area of grinding practice. The section explains where the gaps are in the science of grinding by interpreting the results shown and explained in Sects. 6.2 and 6.3 of this chapter. The first part of the gap analysis focuses on models associated with chip formation, while the second part focuses on tribological interactions associated with ploughing and sliding.

Interaction models associated with chip formation in machining were reviewed and the following observations made:

1. Models associated with understanding the mechanics of cutting with single point tools are very well documented and are reviewed by [87–92]. The common assumptions associated with these models include: orthogonal cutting is dominant, a shear plane exists, the shear plane angle takes a value such that the work done is a minimum, the shear strength along the shear plane is constant, continuous chip formation is apparent, the behaviour of the material is independent of the rate of deformation, the effects of temperature are negligible, and the material properties do not change during deformation. However, depending on the size of the undeformed chip, these models may not be applicable due to the 'size effect' that is prevalent in grinding processes (the size effect is stated as the increase in specific cutting energy (energy required to remove a unit volume of work material) owing to an increase in energy associated with ploughing and sliding (non-chip making interactions) as the uncut

chip thickness decreases for a cutting tool of finite edge sharpness). Therefore, further studies will be required to test the validity of these models. Models explained in this chapter may be applicable as they account for the size effect in grinding. In this context, models can be classed as blends of physical, mathematical, and computational solutions;

2. Chemical models appear to be absent from the classical models. The effect of grain, workpiece and bond chemistry should be considered significant especially when one considers the significance of the size effect on chip formation;
3. Effects of shear strain rates and shear strains on the 'size effect' in grinding have not been thoroughly investigated. Such studies could yield insights into optimizing kinematics conditions, and developing new products that exploit the effects of very high shear strains on chip formation, i.e. grains that fracture with rake angles designed to induce very thin and long chips that can be captured by large pores that accommodate them;
4. Reducing the magnitude of shear stress as a function of chip size is a technical challenge that does not appear to have been addressed in the form of any models. This may be the domain of tribochemistry where mechanical-chemical models need to be developed in order to understand how to design improved products and modify the grinding process. The gaps in the literature exist owing to the lack of scientific understanding of the 'size effect'. Gaps may be filled by combining machining and material structure models with tribochemical effects;
5. Treatment of the 'size effect' in machining literature certainly shows that there is a lack of models describing how surface treatments or the effects of adsorbed chemical species might affect the activation of slip planes in the shear zone. There are no reported models that describe how these complex reactions affect chip forming at the microscopic scale. Indeed, there are no models describing the effect of shear stresses and compressive stresses on the size of the shear plane with regard to chemical effects. Again, tribochemical models are lacking in these areas;
6. The effects of very large plastic strains on chip formation and ramifications for abrasive product design and grinding system performance are not very well understood. This is unfortunate since the plastic strain at fracture is heavily influenced by compressive stresses set up in the shear zone. Models shown in the literature appear to be limited to shear strains in the range of 1–8 (In grinding, shear strains range from 4 to 20);
7. Traditionally, the amount of specific energy as a function of undeformed chip thickness is well understood. However, according to Kececioglu [93], the specific energy is better described by considering it as a function of shear plane area because it is a function of: (i) the mean normal stress on the shear plane; (ii) the shear volume of the shear zone; (iii) The strain rate in the shear zone; (iv) the temperature of the shear plane; and (v) the degree of strain hardening before cutting. Clearly, models will need to be developed in this area to understand chip formation in grinding;

8. Zhang and Bagchi [94] propose the use of a void nucleation model in understanding the 'size effect' in chip formation. However, there are no models that describe how to prevent the re-welding of microcracks in such thin shear zones. Again, filling a gap in the application of suitable tribochemical models may yield benefits in the design of products when considering the role of surface treatments or chemisorbed species on products during chip formation;
9. It is noted that inhomogeneous microstrains may prevent chip formation at extremely low undeformed chip thickness levels. The challenge here is to promote homogeneous microstrains to aid chip formation. Models need to be developed in this regard to understand how to create chips and how they aid product design;
10. There is no mention of the Rebinder effect in any discussion on chip formation, and certainly no models to describe it (The Rebinder effect is the improvement of surface properties of a material caused by a reduction in surface energy). This area of modeling should be linked to tribochemical effects and how it relates to enhancing grinding system performance and product design; and
11. A paper by Duwell and McDonald of the 3 M Company published in Duwell and MacDonal [95] appears to have recognized the complexity of grinding process interactions (mechanical, chemical, thermal). The authors decided to take an empirical approach to abrasive product evaluation in grinding since the late 1950s. Later papers appear to confirm this approach and are shown in the reference section [96–103].

Interaction models associated with grit ploughing and sliding were reviewed and the following observations made:

1. Ploughing and sliding models have been reviewed and appear to be well understood for very simple tribological interactions and should be applied to simple grinding situations to test their validity. However, models are required for more complex situations such as grinding where the following information is required: (i) the true area of contact; (ii) the number of instantaneous contacting points; (iii) the arrangement of contacts with the nominal area of contact; (iv) and the time required to create new points of contact. It may be possible to use simple models that incorporate limitations imposed by certain grinding conditions that may be classified as 'special cases'. However, more complex models may enhance the ability to develop better abrasive products;
2. Thermoelastic behaviour is shown to be responsible for sliding interactions, but models that describe complex situations associated with stick-slip and static contacts are less common. The role of contaminant films are critical in reducing or increasing the coefficient of friction and models are required to describe the role of adhesive bonding and reducing surface energy. There appears to be little modeling conducted related to chip and bond interactions, especially in abrasive machining where sliding speeds are much higher than tribological testing conditions;
3. Sliding friction models that account for the effect of debris generation at high speeds especially for the purpose of chip making (chips clearing from the

grinding zone) are not available. This is an area that may be particularly fruitful for abrasive product design, such as the design of pore networks that capture certain forms of chips, or the formation of grooves on abrasive grains to maintain a pathway for chips to enter pore networks. Surface treatments may aid in chip gelling, which may be useful although not investigated. Few models are available to test these conditions;

4. Temperature models for sliding are well developed and may be used to calculate heat at the interfaces between workpiece, chip, abrasive grain and bond. The temperatures generated and the flow of heat may be controlled by the shape of the grains and may lead to the design of products where a particular shape of grain of known conductivity/diffusivity can be used to form a composite wheel designed to take heat away from the contact zone. These models do not appear to account for heat flow associated with ploughing;
5. In addition to sliding models and their applicability to improving the chip formation process in grinding, there are a lack of models that describe tribochemical effects and the type of lubrication required for a particular chip-forming situation (solid, liquid or gaseous lubrication); and
6. Tribochemistry is a very important aspect of lubrication as well as unlubricated grinding conditions. One of the most comprehensive treatments of tribochemistry is the text by Heinicke [104]. Heinicke identifies a number of sub-topics of tribochemistry, including tribodiffusion, tribosorption, tribodesorption, tribореactions, tribooxidation, tribocatalysis, etc. Tribochemistry is a very challenging discipline, since multiple chemical processes can be occurring simultaneously in lubricated tribosystems and models that describe these complex situations are lacking. Adapting existing sliding and ploughing models or developing new sliding and ploughing models may further enhance how chip and bond interactions can be manipulated to improve the performance of existing abrasive products and/or develop new products and develop new applications.

Interaction models associated with other frictional interactions (chip/bond, chip/work, bond/work) were reviewed and the following observations made:

1. There appears to be a lack of models that describe chip-bond interactions, chip-workpiece interactions and bond-workpiece interactions in the open literature especially when operating at speeds associated with grinding; and
2. Tribological models of sliding for systems such as glass-on-metal, metal-on-metal, polymer-on-metal and other material sliding systems could be adapted to describe slow-speed interactions in areas such as lapping, honing and polishing. However, there is a need to understand these interactions at intermediate and high speeds in order to apply them to higher speed grinding processes. Adapting existing sliding and ploughing models to operate at higher speeds or developing new sliding and ploughing models may further enhance how chip and bond interactions can be manipulated to improve the performance of existing abrasive products and/or develop new products and develop new applications. In this respect, further studies are required to identify tribological models that could effectively describe chip and bond interactions;

On further inspection of the various cutting and sliding models, no account is taken of the following interactions and are identified as gaps in the model (the following are not fundamental process interactions, but are consequences of process interactions, such as that between the grit and the workpiece): (1) initiation modes of abrasive grain failure—could be due to small amount of attritious wear, poor thermal shock resistance, chemical reactions with bond and workpiece, coolant reactions, eutectic reactions, chemical wear of grain, low fracture toughness of grain, cracks induced in abrasive microstructure; (2) completion modes of abrasive grain failure—could be due to grain pull-out, poor thermal shock resistance, reactions with chemistry of coolant/workpiece; (3) initiation modes of abrasive grain and bond failure—could be due to bond material subjected to too high tangential and normal forces, heat transfer through grain to bond determined by grinding power intensity and thermal energy partitions, grain-bond interfacial activity, bond-workpiece friction initiated by grain wear, large scale fracture of grains; (4) completion modes of abrasive grain and bond failure—could be due to grain release from bond, grain composite (collection of grains) released from the bond also known as 'wheel surface collapse', bond fracture due to erosion or corrosion of bond, fractures in the bond due to heat treatment; and (5) initiation modes of failure initiated through the bond—could be due to poor bond and grain adhesion, thermal expansion mismatch between bond and grain, poor thermal shock resistant bonds, microcracking in bonds, crack propagation from grain to bonding phase. It is suggested that existing models should be augmented by additional models to quantify interaction processes in the grinding zone. It is predicted that doing so would yield a better understanding of abrasive product performance, on an application-by-application basis.

6.5 Summary of Research Recommendations

In summary, the following recommendations are made:

1. Models describing chip formation and models that explain tribological interactions at grinding length scales should be validated and compared to traditional cutting and sliding models. As an example, an initial study could be performed to compare known force and shear plane models developed for single point cutting tools with positive rake angles to that of abrasive grains that predominantly have negative, zero, and positive rake angles. This could be achieved by using a single grain platform by measuring forces and visualizing in-process and post-process shear plane angles to compare and contrast predicted and actual forces, shear plane angles, friction coefficients, and other useful information that characterize the grinding process in terms of frictional interactions along rake, clearance and shear faces/planes. Models that can be compared with experimental data have been developed by research workers such as Ernst and Merchant, Merchant, Stabler, Lee and Shaffer, and Hucks;

It should be noted that further studies be conducted to investigate the applicability of using finite element models to describe specific grinding applications;

2. Shear strain and strain rate models that encompass size effects should be developed. As an example, models could be developed that relate strain and strain rates in terms of the nature of the lamellar spacing from a microstructural viewpoint rather than lamellar spacing alone. Experimental procedures need to be developed that prove or refute the existence of the size effect in terms of identifying the dynamic interactions between workpiece materials, abrasive grains and bonding systems;
3. Size effect dominated chip formation models should be developed that account for tribochemical and microstructural effects, thereby extending physical models of crack formation in materials developed by Argon et al. [105] and Anderson [106];
4. Very large plastic strain models should be developed to explain chip formation by microfracture;
5. The effects of surface treatment should be modeled as a way to describe chip formation due to the size effect, where the size effect is explicitly described as a function of geometry of the cutting tool, its geometry relative to the depth of cut, and the microstructural condition of the workpiece material, i.e., mapping the relationship between geometrical and microstructural features and ease or difficulty in forming a chip thereby extending the work of Argon et al. [105] and Anderson [106];
6. Ploughing and sliding models should be extended to describe complex tribological conditions such as abrasive machining. Models developed by Challen and Oxley and Samuels on ploughing should be adopted and compared with experimental grinding conditions;
7. Sliding friction models should be developed that account for debris generation, chip-workpiece contact and bond-workpiece interactions;
8. Tribochemical models should be developed that predict the performance of lubricants and coolants during grinding processes. Thermal models should be used to control the flow of heat in the contact zone. Thermal models exist for single and multi-point tools and grinding wheels, but do not appear to be used in the course of product development by relating thermal conditions with dynamic material conditions of the abrasive;
9. Gaps identified in cutting and sliding models include: initiation and completion modes of abrasive grain failure; initiation and completion modes of abrasive grain and bond failure; and initiation and completion of modes of failure that act through the bonding system, and models that explain wheel surface collapse. These models can be further developed to include interactions involving multiple contact points between abrasive grains, bonds, chips, workpiece material, and fluids;
10. Models that provide connectivity between microscopic interactions and macroscopic interactions should be developed. In addition to this, models that relate models at different length scales to grinding performance measures should also

be developed. Techno-economic models also need to be developed, i.e. linking cost per component models with micro and macroscopic interaction models would be most useful to product design and selection;

11. Specific models that describe the microscopic interactions should be identified from the literature and applied in the laboratory and compared with observations using a variety of test platforms;
12. Model development should be prioritized by focusing on models that have been developed for micromachining (considering size effects) and applied to grinding conditions. Thereafter, models should be developed that explain the role of bond and chip interactions and how these interactions affect product design and grinding process understanding. Are there size effects associated with these interactions? If so, they should be developed with a view to developing products that exploits that knowledge; and
13. Gap analysis studies should be extended to continue to identify applicable models published in the academic literature and potential models described in patents and sales literature provided by manufacturers of abrasives and abrasive products.

The conclusions drawn from this study show that further work is needed to connect 'size effect' models to grinding models in order to understand grinding system dynamics and to develop products based on size effect cutting, ploughing, and sliding interactions. The identified gaps in existing models are associated with initiation and failure of the bonding system and abrasive grains and their interaction with workpiece materials and chips. Gaps in the models should be filled by identifying mechanisms and potential models that adequately describe the observed gaps. This chapter identifies areas of tribology that may contribute to sliding interactions and it is stated that further work is required to review and apply applicable fretting, corrosion, erosion, fatigue, creep, stress corrosion models and other applicable models that describe sliding interactions between abrasive grain, workpiece, bonding systems, and chips.

In conclusion, it is stated that the gap analysis should be completed and that the newly developed models of those identified gaps be proven, or refuted, through rigorous experimentation, initially by understanding the effects of grit geometry and sharpness on chip formation. Further identification of gaps in the area of grinding science could be achieved by building an experimental apparatus that visualizes the process interactions together with enhanced measurement techniques so that thermo-mechanical interactions for specific grain-work systems can be explored.

Acknowledgments The author acknowledges with thanks the permission to reproduce a selection of figures and tables of data published by Woodhead Publishing, Cambridge, UK. The figures and tables of data were used from the publication: M. J. Jackson and J. S. Morrell, 'Tribology in Manufacturing', Chapter 5, pp 161–242, published in Jackson and Morrell [31]. *ISBN 0 85709 114 X and ISBN-13: 978 0 85709 114 7.* The author of this work also thanks Springer publishers for permission to reproduce and adapt Sects. 6.2 and 6.3 from the work entitled,"Tribology of Machining", *(Published under Springer license number: 3412871241727, June 20, 2014)* published in,"Tribology in Manufacturing Technology", Edited by J. P. Davim, pp. 67–02, Heidelberg, Germany, 2012. *ISBN 978-3-642-31682-1.*

References

1. Backer WR, Marshall ER, Shaw MC (1952) Trans ASME 74:61
2. Shaw MC (1952) J Franklin Inst 254:109
3. Heidenreich RO, Shockley W (1948) Report on strength of solids. Phys Soc Lond 57
4. Ernst HJ, Merchant ME (1941) Trans Am Soc Met 29:299
5. Merchant ME (1945) J Appl Phys 16:318–324
6. Piispanen V (1937) Teknillinen Aikakaushehti (Finland) 27:315
7. Merchant ME (1950) Machining theory and practice. Am Soc Met 9:5–44
8. Barrett CS (1943) Structure of Met. McGraw Hill Co, New York, p 295
9. Bridgman PW (1952) Studies in large plastic flow and fracture. McGraw Hill Co, New York
10. Langford G, Cohen M (1969) Trans ASM 62:623
11. Piispanen V (1948) J Appl Phys 19:876
12. Blazynski, TZ, Cole JM (1960) Proc Instn Mech Eng 1(74):757
13. Shaw MC (1950) J AppI Phys 21:599
14. Walker TJ (1967) PhD Dissertation, Carnegie-Mellon University, PA
15. Walker TJ, Shaw MC (1969) Advances in machine tool design and research. Pergamon Press, Oxford, pp 241–252
16. Usui E, Gujral A, Shaw MC (1960) Int J Mach Tools Res 1:187–197
17. Vyas A, Shaw MC (1999) Trans ASME-J Mech Sci 21(1):63–72
18. Eugene F (1952) Ann CIRP 52(11):13–17
19. Shaw MC (1980) Int J Mech Sci 22:673–686
20. Kwon KB, Cho DW, Lee SJ, Chu CN (1999) Ann CIRP 47(1):43–46
21. Eyring H, Ree T, Harai N (1958) Proc Nat Acad Sci 44:683
22. Eyring H, Ree T (1961) Proc Nat Acad Sci 47:526–537
23. Eyring H, Jhon MS (1969) Significant theory of liquids. Wiley, New York
24. Doyle ED, Horne JG, Tabor D (1979) Frictional interactions between chip and rake face in continuous chip formation. Proc R Soc Lond A 366:173–187
25. Horne JG, Doyle ED, Tabor D (1978) Direct observation of the contact and lubrication at the chip-tool interface. In: Proceedings of the first international conference on lubrication challenges in metalworking and processing. IIT Research Institute, Chicago, USA, June 1978, pp 1–6
26. Madhavan V (1993) School of industrial engineering. MS thesis, Purdue University, West Lafayette, Indiana
27. Ackroyd B (1999) School of industrial engineering. PhD thesis, Purdue University, West Lafayette, Indiana
28. Robinson GM (2007) Mixed scale machining with nanostructured coated cutting tools. PhD thesis, Purdue University, West Lafayette, Indiana
29. Hwang J (2005) School of industrial engineering. PhD thesis, Purdue University, West Lafayette, Indiana
30. Lee S (2006) School of industrial engineering. PhD thesis, Purdue University, West Lafayette, Indiana
31. Jackson MJ, Morrell JS (2011) Tribology in manufacturing, Chap. 5. In: Davim J (ed) Tribology for engineers: a practical guide'. Wood Head Publishing, Cambridge, UK, pp 161–242
32. Young WC (1989) Roark's formulas for stress and strain, 6th edn. McGraw-Hill, New York
33. Greenwood JA, Williamson JBP (1966) Contact of nominally flat surfaces. Proc R Soc Lond A 295:300–319
34. Whitehouse DJ, Archard JF (1970) The properties of random surfaces of significance in their contact. Proc R Soc Lond A 316:97–121
35. Hirst W, Hollander AE (1974) Proc R Soc Lond A 233:379
36. McCool J (1986) Comparison of models for the contact of rough surfaces. Wear 107:37–60

37. Greenwood JA (1992) Problems with surface roughness. In: Singer IL, Pollock HM (eds) Fundamentals of friction: macroscopic and microscopic processes. Kluwer, Dordrecht, pp 57–76
38. Song JF, Vorburger TV (1992) Surface texture. In: Friction, lubrication, and wear technology, ASM handbook, vol 18, 10th edn. ASM International, Materials Park, pp 334–345
39. Burton RA (1980) Thermal deformation in frictionally-heated systems. Elsevier, Lausanne, p 290
40. Ferrante J, Bozzolo GH, Finley CW, Banerjea A (1988) Interfacial adhesion: theory and experiment. In: Mattox DM, Baglin JEE, Gottschall RJ, Batich CD (eds) Adhesion in Solids. Materials research society, Pittsburgh, pp 3–16
41. Buckley DF (1981) Surface effects in adhesion, friction, wear, and lubrication. Elsevier, New York, pp 245–313
42. McClelland GM, Mate CM, Erlandsson R, Chiang S (1988) Direct observation of friction at the atomic scale. In: Mattox DM, Baglin JEE, Gottschall RJ, Batich CD (eds) Adhesion in solids. Materials Research Society, Pittsburgh, pp 81–86
43. McClelland GM, Mate CM, Erlandsson R, Chiang S (1987) Phys Rev Lett 59:1942
44. Thompson PA, Robbins MO (1990) Origin of stick-slip motion in boundary lubrication. Science 250:792–794
45. Robbins MO, Thompson PA, Grest GS (1993) Simulations of nanometer-thick lubricating films. Mater Res Soc Bull XVIII(5):45–49
46. Landman U, Luetke WD, Burnham NA, Colton RJ (1990) Atomistic mechanisms and dynamics of adhesion, nanoindentation, and fracture. Science 248:454–461
47. Belak J, Stowers JF (1992) The indentation and scraping of a metal surface: a molecular dynamics study. In: Pollock HM, Singer IL (eds) Fundamentals of friction: macroscopic and microscopic processes. Kluwer, Dordrecht, pp 511–520
48. Pollock HM, Singer IL eds (1992) Fundamentals of friction: macroscopic and microscopic processes. Kluwer, Dordrecht, p 621
49. Wheeler DR (1975) The effect of adsorbed chlorine and oxygen on the shear strength of iron and copper junctions, NASA TN D-7894
50. Akhmatov AS (1939) Some items in the investigation of the external friction of solids, Trudy Stankina. In: Kragelski IV (ed) (1965) Friction and wear, Butterworths, London, p 159
51. Sikorski ME (1964) The adhesion of metals and factors that influence it. In: Bryant PJ, Lavik L, Salomon G (eds) Mechanisms of solid friction. Elsevier, Amsterdam, pp 144–162
52. Rabinowicz E (1992) Friction coefficients of noble metals over a range of loads. Wear 159:89–94
53. Campbell WE (1940) Remarks printed in proceedings of M.I.T. conference on friction and surface finish. MIT Press, Cambridge, p 197
54. Israelachvili JN (1992) Adhesion, friction, and lubrication of molecularly smooth surfaces. In: Pollock HM, Singer IL (eds) Fundamentals of friction: macroscopic and microscopic processes. Kluwer, Dordrecht, pp 351–381
55. Moore DF (1975) Principles and applications of tribology. Pergamon Press, Oxford, p 152
56. Kosterin JI, Kraghelski IV (1962) Rheological phenomena in dry friction. Wear 5:190–197
57. Kragelski IV (1965) Friction and wear. Butterworths, London, p 200
58. Bowden FP, Tabor D (1986) The friction and lubrication of solids. Clarendon Press, Oxford
59. Kudinov VA, Tolstoy DM (1986) Friction and oscillations. In: Kragelski IV (ed) Tribology handbook. Mir, Moscow, p 122
60. Bartenev GM, Lavrentev VV (1981) Friction and Wear of Polymers. Elsevier, New York, pp 53–61
61. Rabinowicz E (1965) Friction and wear of materials. Wiley, New York, p 69, 89, 99–102
62. Black PH (1961) Theory of metal cutting. McGraw-Hill, New York, pp 45–72 (Chap. 5)
63. Mulhearn TO, Samuels LE (1962) Wear 5:478
64. Hokkirigawa K, Kato K (1988) An experimental and theoretical investigation of ploughing, cutting and wedge formation during abrasive wear. Tribol Int 21(1):51–57

65. Challen JM, Oxley PLB (1979) An explanation of the different regimes of friction and wear using asperity deformation models. Wear 53:229–243
66. Suh NP (1986) Tribophysics. Prentice-Hall, Englewood Cliffs, pp 416–424
67. Bridgman PW (1931) The physics of high pressure. Macmillan Press, New York
68. Kragelskii IV, Dobychin MN, Kombalov VS (1982) Friction and wear calculation methods. Pergamon Press, Oxford, pp 178–180
69. Blok H (1963) The flash temperature concept. Wear 6:483–494
70. Blok H (1937) General discussion on lubrication. Inst Mech Eng 2:222
71. Jaeger JC (1942) J Proc R Soc N South Wales 76:203
72. Cowan RS, Winer WO (1992) Frictional heating calculations. In: Friction, lubrication, and wear technology, ASM handbook, vol 18, 10th edn. ASM International, Materials Park, pp 39–44
73. Kuhlmann-Wilsdorf D (1987) Demystifying flash temperatures I. Analytical expressions based on a simple model. Mater Sci Eng 93:107–117
74. Dow TA, Stockwell RD (1977) Experimental verification of thermoelastic instabilities in sliding contact. J Lubr Technol 99(3):359
75. Griffioen JA, Bair S, Winer WO (1985) Infrared surface temperature in a sliding ceramic-ceramic contact. In: Dowson D et al (eds) Mechanisms of surface distress. Butterworths, London, pp 238–245
76. Quinn TFJ, Winer WO (1987) An experimental study of the 'hot spots' occurring during the oxidational wear of tool steel on sapphire. J Tribol 109(2):315–320
77. Enthoven JC, Cann PM, Spikes HA (1993) Temperature and scuffing. Tribol Trans 36 (2):258–266
78. Wills JG (1980) Lubrication fundamentals. Marcel Dekker, New York
79. Klaus EE, Tewksbury EJ (1984) Liquid lubricants. In: Booser ER (ed) The handbook of lubrication (Theory and practice of tribology), vol II. CRC Press, Boca Raton, pp 229–254
80. Sanchez-Rubio M, Heredia-Veloz A, Puig JE, Gonzalez-Lozano S (1992) A better viscosity-temperature relationship for petroleum products. Lubr Eng 48(10):821–826
81. Ramesh KT, Clifton RJ (1987) A pressure-shear plate impact experiment for studying the rheology of lubricants at high pressures and high shear rates. J. Tribal. 109:215–222
82. Raimondi AA (1968) Analysis and design of sliding bearings, Chap. 5 in standard handbook of lubrication engineering. McGraw-Hill, New York
83. Hall AS, Holowenko AR, Laughlin HG (1961) Lubrication and bearing design, in Machine design, Schaum's outline series. McGraw-Hill, New York, p 279
84. Hutchings IM (1992) Tribology—friction and wear of engineering materials. CRC Press, Boca Raton, p 65
85. Briscoe BJ, Stolarski TA (1993) Friction, Chap. 3 in characterization of tribological materials. In: Glaeser WA. Butterworth Heinemann, Boston, pp 48–51
86. Glaeser WA, Dufrane KF (1978) New design methods for boundary lubricated sleeve bearings. Machine Design, April 6, pp 207–213
87. Zorev NN (1966) Metal Cutting Mechanics. Pergamon Press, Oxford, England
88. Komanduri R (1993) NSF Report on US Contributions to Machining and Grinding Research in the 20th Century, Oklahoma, USA
89. Trent E, Wright P (2000) Metal Cutting, 4th edn. Butterworth Heinemann, New York
90. Shaw MC (2005) Metal cutting principles, 2nd edn, Oxford University Press, New York
91. Astakov V (2006) Tribology of metal cutting, Elsevier, New York
92. Atkins A (2009) The science and engineering of cutting, Butterworth Heineman, New York
93. Kececioglu D (1960) Trans. ASME-J. Eng for Industry, 82, 79–86
94. Zhang B, Bagchi A (1994) Trans. ASME- J. of Eng for Industry, 116, 289
95. Duwell EJ, McDonald WJ (1961) Some factors that affect the resistance of abrasive grits to wear. J Wear 4:371–383
96. Duwell EJ (1990) Ceramic Aluminium Oxide—a new abrasive grit for coated and bonded abrasive tooling, SME paper MS90-304. In: International manufacturing technology conference. Chicago, Illinois

97. Duwell EJ, McDonald WJ (1971) Performance and evaluation of coated abrasives in heavy duty grinding operations, SME paper MR . In: International grinding conference. Dearborn, Michigan, pp 71–412
98. Duwell EJ, Cosmano R, Abrahamson G (1984) Dynamics of grinding with coated abrasives, SME paper MR84-546. In: International grinding conference, August 1984. Fontana, Wisconsin
99. Duwell EJ, Gagliardi JJ (1990) Belt grinding with ceramic oxide aluminium oxide, SME paper MR90-543. In: International grinding conference, October 1990. Dearborn, Michigan
100. Gagliardi JJ, Duwell EJ (1989) Coated abrasives made with abrasive grit clusters for constant performance surface finishing, SME Paper MR89-139. In: Deburring and surface conditioning conference, February 1989, San Diego, California
101. Hong IS, Duwell EJ (1975) Centerless grinding with coated abrasive belts, SME paper MR 75-616. In: International grinding conference. Dearborn, Michigan
102. Yoon SC Laramie HA (1990) Use of sintered ceramic oxides in vitrified bonded wheels, SME paper EM90-360. In: International manufacturing technology conference. Chicago, Illinois
103. Heinicke G (1984) Tribochemistry. Carl Hanser Verlag, Munich, p 446
104. Bhushan B, Gupta BK (1991) Handbook of Tribology. McGraw-Hill, New York pp 5–11, pp 5–12
105. Argon AS, Im J, Safoglu R, 1975, Metallurgical transactions, 6A, 825
106. Anderson TL (1991) Fracture mechanics, CRC Press, Florida